Aus dem Zentrum für Zahnmedizin

Abteilung für Oralchirurgie und Zahnärztliche Röntgenologie

Medizinische Fakultät Charité – Universitätsmedizin Berlin

DISSERTATION

Characterization of the osteopetrotic Clcn7-/- mouse mutant rescued by osteoclast-specific expression of ClC-7

zur Erlangung des akademischen Grades

Doctor medicinae dentariae (Dr. med. dent.)

vorgelegt der Medizinischen Fakultät

Charité – Universitätsmedizin Berlin

von

Chayarop Supanchart

aus Chiangmai, Thailand

Gutachter: 1. Prof. Dr. P. A. Reichart

2. Prof. Dr. Dr. H. Schliephake

3. Priv.-Doz. Dr. Dr. E. Nkenke

Datum der Promotion: 27. März 2009

Abstract

Bone quality is a consequence of simultaneous functions of bone formation cells or osteoblasts and bone resorption cells or osteoclasts. Imbalance function of these cells disturbs bone remodeling and consequently leads to pathological bone diseases. Complete loss of function or insufficient differentiation of osteoclasts causes excessive bone density or osteopetrosis. Intracellular transmembrane protein chloride channel-7 (ClC-7), which is highly expressed in osteoclasts is required for electroneutralization during bone degradation. Complete depletion of the protein gives rise to autosomal recessive osteopetrosis (ARO) in humans and osteopetrosis phenotype in mice. Moreover, in approximately 70% of autosomal dominant osteopetrosis type II (ADO II) patients, heterozygous mutations of *CLCN7* are identified. Because ClC-7 structure is dimmers, in which each of two subunits has its own pore, the heterozygous mutations should be encoded for <25% of the entire protein, statistically. However, the mutations' carriers do not express phenotype. The pathogenesis of the disease remains unclear. Hence, the present study was aimed to explain the mechanism of the diseases relevant to ClC-7 expression. **Methods**: To answer the question, three transgenic mouse lines were constructed by genome-integration of ClC-7 cDNA which is under control of osteoclast-specific Acp5 (Trap) promoter. Heterozygous mice (*Clcn7*+/- Tg+) were mated. Then, *Clcn7*-/- Tg+ mice could be generated in the second generation. Accordingly, ClC-7 could be expressed partially. Bone phenotypes of the transgenic mice with different *Clcn7* genotypes were investigated histomorphologically. Structural and cellular parameters were compared between the genotypes, and groups statistically (independent paired *t-test*). ClC-7 and other osteoclast specific proteins were also determined *in situ* using the immunofluorescent technique. mRNA and protein extracted from osteoclasts in vitro were examined by quantitative PCR and Western blot analysis, respectively. **Results**: The *Clcn7* knockout mice and F7 showed severe osteopetrosis phenotype, whereas F1 and F3 had different degrees of bone density. F1 rescue mice had mild osteopetrosis phenotype, while F3 rescue mice and heterozygous mice displayed insignificant bone phenotype. Osteoclast and osteoblast numbers were reversely associated with the degree of bone density. Interestingly, Clcn7 mRNA and ClC-7 expressed very low in F1 and F3. Moreover, ClC-7 expression in F3 was 5.70±1.4%, while the average value in F1 was decreased to 2.51±0.89% of control signals. **Conclusion**: The expression of ClC-7 is associated with the degrees of bone density. Low degree expression of ClC-7 can rescue the osteopetrosis phenotype. The reduced bone resorption function due to impaired ClC-7 prolongs the bone remodeling process and results in mild osteopetrosis. Recessive pattern of the inheritance of the mutated gene leads to severe osteopetrosis in humans

and mice, whereas heterozygous mutations cannot affect osteopetrosis phenotype in mice. Thus, the pattern of genotype-phenotype relationship would be different between species. The study would be meaningful for genetic diagnostics and the prediction of severity of the disease. Furthermore, F1 mice displayed a phenotype very similar to ADO II, thus the F1 mice would be a beneficial model for treatment trials of the disease as well as for the study of osteoporosis.

Keywords*: bone density, bone remodeling, chloride channel, histomorphometry, osteoclast, osteopetrosis, transgene, mice model*

Zusammenfassung

Die Struktur des Knochens wird bestimmt durch ein komplexes Zusammenspiel von Osteoblasten, die Knochen aufbauen, und Osteoklasten, die Knochen abbauen. Durch ein Ungleichgewicht dieses Prozesses resultieren Erkrankungen mit veränderter Knochendichte. Die Osteopetrose ist eine generalisierte osteosklerotische Erkrankung, die durch Verlust der Osteoklastenfunktion bzw. Defekte der Osteoklastendifferenzierung entstehen. Das Chloridkanal-Protein ClC-7, das in Osteoklasten stark exprimiert ist, hat eine wichtige Funktion bei der Säuresekretion der Osteoklasten, welche für die Resorptionstätigkeit essentiell ist. Es ist daher folgerichtig, dass ein völliger Verlust des Proteins die infantil maligne Osteopetrose in Mensch (ARO) bzw. einen letalen Osteopetrose-Phänotyp in der Maus zur Folge hat. Darüber hinaus werden in ungefähr 70% der Fällen von dominanter Osteopetrose (ADOII) heterozygote Mutationen im Gen für ClC-7 identifiziert, die statistisch die Menge an funktionellen ClC-7 Dimeren maximal auf 25% reduzieren sollten. Heterozygote Träger rezessiver Mutationen haben keinen Phänotyp. Da es gegenwärtig ungeklärt ist, ab welchem Grad von Funktionsverlust von ClC-7 die Osteoklastenfunktion eingeschränkt wird, wurden in dieser Studie verschiedene Mauslinien mit unterschiedlich starkem ClC-7 Expressionsniveau untersucht. **Methoden**: Drei Mauslinien (F1, F3, und F7), die ein transgenes Konstrukt, das aus dem Osteoklasten-spezifischen Acp5 (Trap)-Promoter und der ClC-7 cDNA besteht, stabil im Genom integriert haben, wurden mit Clcn7+/- Mäusen verpaart, so dass in der zweiten Generation Clcn7-/- Tg+ Tiere entstanden, bei denen der Funktionsverlust des Clcn7-Gens durch transgene Expression teilweise ausgeglichen wurde. Die Clcn7-/- Tg+ Tiere wurden histomorphometrisch untersucht. Die Strukturparameter und Zellzahlen wurden statistisch (unabhängiger gepaarter *t-Test*) zwischen den Genotypen und den Linien verglichen. ClC-7 wurde *in situ* im Vergleich mit anderen Osteoklastenproteinen durch Immunofluoreszenz nachgewiesen. Weiterhin wurden Osteoklasten der verschiedenen Mauslinien in vitro kultiviert. mRNA und Proteine wurden extrahiert und durch quantitative PCR und Western-Blot quantifiziert. **Ergebnisse**: Clcn7-/- Mäuse und Clcn7-/- Tg+ Tiere der Linie F7 hatten einen gleich schweren osteopetrotischen Phänotyp, so dass keine transgene Expression vorhanden sein konnte. Diese Linie wurde nicht weiter untersucht. Dagegen wurde die Osteopetrose bei den Linien F1 und F3 deutlich abgemildert, was für eine teilweise Wiederherstellung der Osteoklastenfunktion spricht. F3 Mäuse zeigten eine annähernd normale Knochendichte, während F1 Mäuse eine milde Osteopetrose darboten, die in etwa dem Phänotyp der dominanten Osteopetrose entspricht. Die Anzahl der Osteoblasten und die Anzahl der Osteoklasten korrelierte umgekehrt mit der

Knochendichte. Die Expression von Clcn7 mRNA und Protein war in beiden Linien überraschend niedrig. In F3 wurde die Proteinexpression auf 5,70±1,4 % gemindert, während die Expression in F1 nur 2,51±0,89 % betrug. **Schlussfolgerung**: Die Clcn7-/- Tg+ Tiere der Linie F1 zeigten einen milden Osteopetrose-Phänotyp, der einer autosomal dominanten Osteopetrose nahekommt, während in Linie F3 die Knochendichte durch die transgene Expression von ClC-7 im Clcn7-/- Hintergrund annähernd normalisiert wurde. Damit korreliert die Proteinexpression, die jedoch unter den erwarteten Werten von 25-50% liegt. Dies könnte durch einen Speziesunterschied begründet sein.

Acronym and abbreviation list

µCT	micro-computerized tomogram
ADO	autosomal dominant osteopetrosis
ADOII	autosomal dominant osteopetrosis type 2
ALP	alkaline phosphatase
AMPase	adenosine monophosphatase
ARO	autosomal recessive osteopetrosis
ATF4	activating transcription factor 4
ATP	adenosine triphosphate
ATPase	adenosine triphosphatase
B.Ar/T.Ar	bone density (2-dimension)
BMD	bone mineral density
BSP	bone sialoprotein
CAII	carbonic anhydrase II
cDNA	complementary DNA
c-fms	macrophage colony-stimulating factor 1 receptor
ClC-7	chloride channel 7
Clcn7	chloride channel 7 gene (Mus musculus)
CLCN7	chloride channel 7 gene (Homo sapiens)
Ctl	control
CTR	calcitonin receptor
DEPC	Diethylpyrocarbonate
FGFR2	fibroblast growth factor receptor 2
Gapdh	glyceraldehyde-3-phosphate dehydrogenase
HA	hydroxyapatite
Het	heterozygous
HSCT	haematopoietic stem cell transplantation
ITAM	immunoreceptor tyrosine-based activation motif
KO	knockout
LRP5	lipoprotein receptor-related protein 5
MAR	mineral apposition rate
MCP-1	monocyte chemoattractant protein-1
M-CSF	macrophage colony-stimulating factor
MEA	2-Methoxyethyl acetate
MMA	methyl methacrylate
MMP-9	matrix metalloproteinase 9

mRNA	messenger ribonucleic acid
N.Ob/BS	Osteoblast number
N.Oc/BS	Osteoclast number
NFATc1	nuclear factor of activating T cell c1
O.Ar/B.Ar	Osteoid volume
Ob.S/BS	Osteoblast surface
Oc.S/BS	Osteoclast surface
OCN	osteocalcin
ON	osteonectin
OPN	osteopontin
OS/BS	Osteoid surface
OSCAR	osteoclast-specific immunoreceptor osteoclast-associated receptor
Osx	Osterix
PBS	phosphate buffered saline
PCR	polymerase chain reaction
Ppi	inorganic pyrophosphate
Ppiase	inorganic pyrophosphatase
PTH	parathyroid hormone
RANKL	receptor activator of NF-κB ligand
ROI	region of interest
RTA	renal tubular acidosis
Runx2	Runt-related transcription factor 2
TGFβ	transforming growth factor β
TNF	tumor necrosis factor
Tr.N	trabecular number
Tr.Sp	trabecular separation
Tr.Th	trabecular thickness
TRAcP5, TRAP	tartrate-resistant acid phosphatase 5
TRAF6	TNF receptor-associating factors 6

Contents

1. Introduction

The skeleton serves as a framework of the body and protects internal organs. Together with the musculature it allows the movement of body parts and the locomotion of the organism. Additionally, bone is a highly mineralized tissue and therefore an important reservoir of essential trace elements such as calcium and phosphate. Calcium, albeit being the most abundant cation in our body, has very low intracellular levels. The resulting gradient between extra- and intracellular calcium levels allow the utilization of this ion as a universal intracellular second messenger [1]. Calcium participates in many physiological functions such as fertilization, synaptic transmission, muscle contraction, as well as blood clot formation. Because of the crucial role of the skeleton in calcium metabolism, many skeletal disorders result in calcium dysregulation.

1.1 **Bone remodeling**

Bone remodeling is a pivotal process that is highly active during growth, but also serves to adjust the bone structure to the mechanical or metabolic needs in adulthood. About 10% of the bone mass are thus resorbed and replaced by newly formed bone per year [2]. This process relies on the coordinated activity of two types of bone cells: osteoblasts and osteoclasts.

1.1.1 Origin and differentiation of osteoblasts

Osteoblasts arise from mesenchymal cells contained in the stroma of bone marrow and from pericytes adjacent to small blood vessels in connective tissue [3-5]. The activation of the Wnt/β-Catenin pathway, fibroblast growth factor receptor 2 (FGFR2), and transforming growth factor β (TGFβ) can regulate the expression of transcription factors which are required for osteoblastic lineage commitment and cellular differentiation.

Runt-related transcription factor 2 (Runx2) is a fundamental transcription factor controlling osteoblastic lineage commitment and differentiation. During endochondral ossification Runx2 starts to be expressed when the chondrocytes in the cartilaginous bone precursor undergo hypertrophy and is essentially present in osteoblasts at all differentiation stages. Consequently, mice lacking Runx2 expression show neither hypertrophic cartilage nor bone [6]. After the mesenchymal cells are decided to be bone lineage cells under the regulation of Runx2, they

sequentially become osteoprogenitor cell, immature osteoblast, and mature or active osteoblasts. Beside Runx2, activation of Osterix (Osx), β-Catenin, and activating transcription factor 4 (ATF4) can mediate osteoblast differentiation from osteoprogenitor cells [7-10]. These transcription factors are required for the expression of osteoblast-related proteins and major extracellular matrix including type I collagen alpha 1 chain, bone sialoprotein, and osteocalcin.

At the active stage, osteoblasts become larger and typically cuboidal. They have a large eccentric nucleus accompanied by prominent rough endoplasmic reticulum and Golgi area. The active osteoblasts secrete bone matrix proteins across apical membrane towards the osteoid seam. Finally, after the osteoid is successfully formed, the osteoblasts are retired and convert to one of three destinations, i.e. 1) become embedded in the bone as osteocytes, or 2) lie on the bone surface as inactive osteoblasts or bone lining cells, or 3) undergo programmed cell death (apoptosis).

A large number of active osteoblasts undergo apoptosis, whereas 10-20% transform into osteocytes[11]. Runx2 and β-catenin/LEF1 are involved in the decision of the osteoblast cell fate. Although the presence of TGF-β can protect the osteoblast from apoptosis, an attenuation of TGF-β signaling tends to increase the rate of osteoblast/osteocyte transformation [12, 13]. On the other hand, the modulation of Runx2 by parathyroid hormone (PTH) or the canonical Wnt pathway can induce osteoblast survival and inhibit transformation into osteocytes [14, 15].

1.1.2 Production and mineralization of the extracellular matrix

At the first step of bone formation, polarized osteoblasts form the non-mineralized part, the so called osteoid by secretion of bone matrix. Most of the bone matrix protein secreted by osteoblasts is collagen type 1. The non-collagenous matrix proteins include e.g. bone sialoprotein (BSP), osteopontin (OPN), and osteocalcin (OCN). After the osteoblasts have formed the osteoid, mineralization is initiated by matrix vesicles which are also released by the osteoblasts. At the beginning of the mineralization stage, the matrix is prepared in vesicles which are 50-200 nanometers in diameter [16]. The vesicles contain adenosine triphosphate (ATP) and the enzyme phosphatases including bone alkaline phosphatase (ALP), adenosine triphosphatase (ATPase), adenosine monophosphatase (AMPase), and inorganic pyrophosphatase (PPiase). These enzymes regulate Ca_2PO_4 production. At the beginning of the mineralization process, the ATP is hydrolyzed by nucleoside triphosphate pyrophosphohydrolase to yield AMP and inorganic

pyrophosphate (PPi). Both AMP and PPi are further hydrolyzed to orthophosphate (PO_4^{3-}) by ALP. Besides the phosphate-producing substances and enzymes, the matrix vesicles contain Annexin V, and Ca^{2+}-binding proteins including BSP, OCN, and osteonectin (ON). Of these proteins only BSP has been shown to promote *in vitro* mineralization [17, 18]. Ca^{2+} is actively transported into the vesicle by Annexin V. When sufficient Ca^{2+} and PO_4^{3-} have accumulated within the vesicles, $CaPO_4$ mineral will begin to precipitate. The regulation of $CaPO_4$ formation is modulated by PPi levels. High levels of non-hydrolyzed PPi (> 1-2 mM) tend to block the formation of $CaPO_4$ [19], whereas lower PPi levels stimulate $CaPO_4$ production [20]. The first product of $CaPO_4$ is non-crystalline (amorphous $CaPO_4$). Under the proper condition, the amorphous $CaPO_4$ will convert to octacalcium phosphate ($Ca_{10}(PO_4)_6(OH)_2$), and then transform into highly insoluble hydroxyapatite (HA). The accumulation of HA can penetrate the vesicle membrane by the assistance of the hydrolytic action of phospholipases. Finally, after the HA leave vesicles, they proliferate and come into contact with collagen fibrils of the surrounding matrix. At this point, the collagens fibrils begin to play a role in the nucleating and orientating of newly formed apatite crystal (mature form of HA).

1.1.3 Origin and differentiation of osteoclasts

Osteoclasts are large, multinucleated cells whose function is mainly to degrade bone. They are derived from haematopoietic stem cells that also give rise of the monocyte/macrophage lineage. Osteoclastogenesis depends on osteoblasts and stromal cells which release two cytokines: receptor activator of NF-κB ligand (RANKL) and macrophage colony-stimulating factor (M-CSF). These cytokines bind to their respective receptors on marrow-derived osteoclast precursors. RANKL binds to RANK, a member of tumor necrosis factor (TNF) receptor family, while M-CSF binds to macrophage colony-stimulating factor 1 receptor (c-fms), a receptor tyrosine kinase. Stimulation of these receptors leads to activation of downstream intracellular signaling pathways initiated by TNF receptor-associating factors 6 (TRAF6). This signaling pathway activates a transcriptional upregulation of nuclear factor of activating T cell c1 (NFATc1) in an early phase of osteoclastogenesis. Beside RANK-TRAF6 cascades, an immunoreceptor tyrosine-based activation motif (ITAM) found in several osteoclast-expressed receptors, e.g. osteoclast-specific immunoreceptor osteoclast-associated receptor (OSCAR), is capable of activating NFATc1 through intracellular calcium signaling. Finally, the activation of NFATc1 governs transcriptions of osteoclast-specific genes such as *cathepsin K* [21], *tartrate-*

resistant acid phosphatase 5 (TRAcP5) [22, 23], *calcitonin receptor (CTR)* [23], *β3 integrin* [24], and *OSCAR* [25].

1.1.4 Maturation of osteoclasts and bone adhesion

The bone resorptive activity of osteoclasts depends on systemic factors such as estrogen, parathyroid hormone (PTH), 1,25$(OH)_2$ Vitamin D_3, etc.. In order to become active, osteoclasts change their polarity. These structural alterations include the formation of a ruffled border and a sealing zone at the plasma membrane facing the bone surface. Osteoclasts can adhere to several substrates; bone, dentin, plastic, as well as glass by the formation of podosomes. The podosome are formed by an F-actin core surrounded by several focal adhesion proteins. αvβ3 integrin is the most abundant adhesion molecule in osteoclasts and acts as a receptor of the podosome core which is responsible for forming a sealing zone for bone resorption. C-Src acts downstream of αvβ3 integrin to regulate the assembly and disassembly of the podosome. C-Src deficient mice have progressive increase of bone mass resulting from a lack of ruffled border[26]. In addition, αvβ3 integrin-deficient osteoclasts cannot organize actin ring[27]. Thus, the formation of ruffled border is especially dependent on reorganization of the actin cytoskeleton and the formation of αvβ3 integrin-containing focal adhesions.

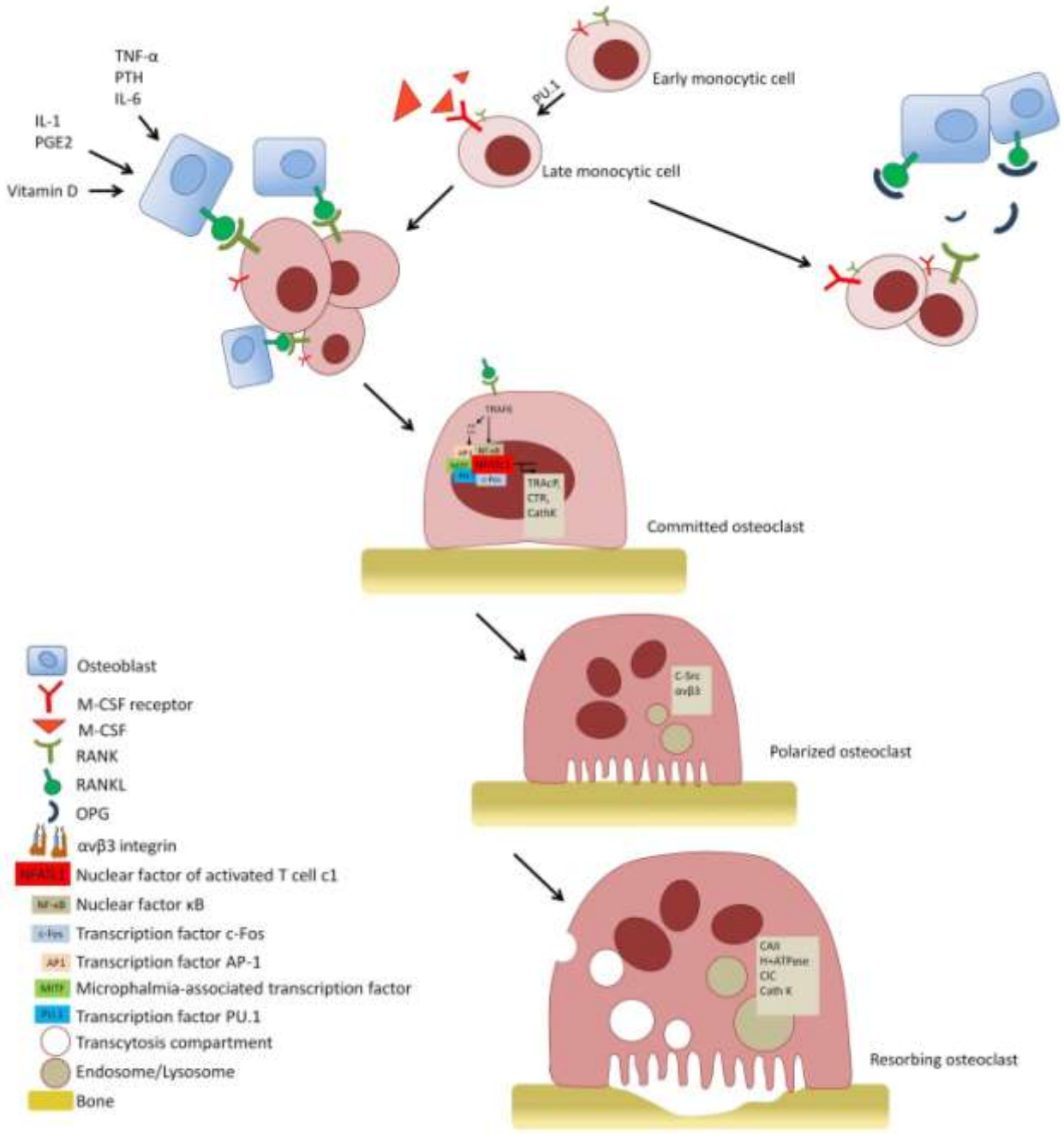

Fig.1 Important factors regulating osteoclast differentiation

1.1.5 Bone resorption by osteoclasts

Once a sealing zone and ruffled border are formed, osteoclasts commence to secrete acid into the growing resorption lacuna. These protons are required a) for the dissolution of the

hydroxyapatite ($Ca_5(PO_4)_3(OH)$) in the bone and b) for the degradation of the organic matrix by acid hydrolases. Protons for the acidification are generated from hydration of carbon dioxide by carbonic anhydrase II (CAII) which is highly expressed within the osteoclast's cytosol [28, 29]. The protons are transported through the vacuolar (v-) type H^+-ATPase complex which resides in the late endosomal/lysosomal compartment and in the ruffled border [30-32]. As a result the extracellular pH drops to levels around 4. By the proton transport a massive electric potential would be formed in the absence of charge compensation by anions. Early investigations already demonstrated the presence of a chloride conductance in osteoclast-derived vesicles [33]. Later it became clear that the chloride channel ClC-7 is highly expressed in osteoclasts and predominantly resides in the ruffled border. ClC-7 deficient mice develop a severe osteopetrosis due to a loss of bone resorption [34]. The intracellular pH during the production of H^+ is maintained by the HCO^-/Cl^- exchanger located at the basolateral membrane [35].

Osteoclasts also have the ability to produce and release proteolytic enzymes which are necessary for degradation of organic constituents of the bone. Among the other cathepsins, cathepsin K expresses dominantly in osteoclasts and is a member of cysteine protease family which is responsible for degradation of collagen type I and other bone proteins. Functional studies revealed that the lack of activity of cathepsin K results in inhibition of resorptive activity by osteoclast and causes an osteopetrosis phenotype [36-38]. Cathepsin K deficiency also causes human pycnodysostosis which is characterized by short stature, osteosclerosis, acroosteolysis, spondylolysis, separated cranial sutures with open fontanels, bone fragility and loss of mandibular angle [39, 40]. Another proteolytic enzyme, MMP-9 is localized in osteoclasts or chondroclasts at the chondro-osseous junction [41]. MMP-9-mutant mice demonstrate an expansion of the zone of hypertrophic chondrocytes in the growth plate.

Tartrate-resistant acid phosphatase (TRAP; TRAcP5) is synthesized as an inactive latent proenzyme. The processing to the mature enzyme requires the activity of a cysteine protease which has the ability to cleave the 34 kDa- proenzyme into the two-subunit active form [42]. Under normal conditions, the rate of TRAcP5 synthesis by osteoclasts mirrors the number of osteoclasts and thus the rate of bone resorption [43]. Since the demonstration that the enzyme is resistant to the inhibitory effect of tartrate, TRAcP has been widely used as a cytochemical marker of osteoclasts and their precursors for many years [44-47]. Histologically, TRAcP has also been demonstrated in lung and spleen macrophages [48]. In several studies immunochemistry or RT-PCR techniques have also revealed that TRAcP is expressed in cells

belonging to osteoclast/macrophage lineage [49-51]. Electron microscopic studies revealed that TRAcP is localized in lysosomes, vacuoles, and the ruffled border of osteoclasts [52-55]. Other studies argued that TRAcP resides in the ruffled border [56]. Furthermore, the presence of TRAcP in the transcytosis pathway depends on activity of cells [51, 57]. These studies suggested that TRAcP might play a pivotal role in bone resorption. Mice lacking TRAcP show disrupted endochondral ossification and mild osteopetrosis [58], while transgenic mice with overexpression of TRAcP showed an increase bone resorption and mild osteoporosis [59]. The role of TRAcP in intracellular bone degradation is still unspecified. Possible substrates of TRAcP are ATP [60], mannose-6 –phosphate [61], or osteopontin [62]. It is interesting to note that serum TRAcP levels are elevated in patients with autosomal dominant osteopetrosis type 2 (ADOII).

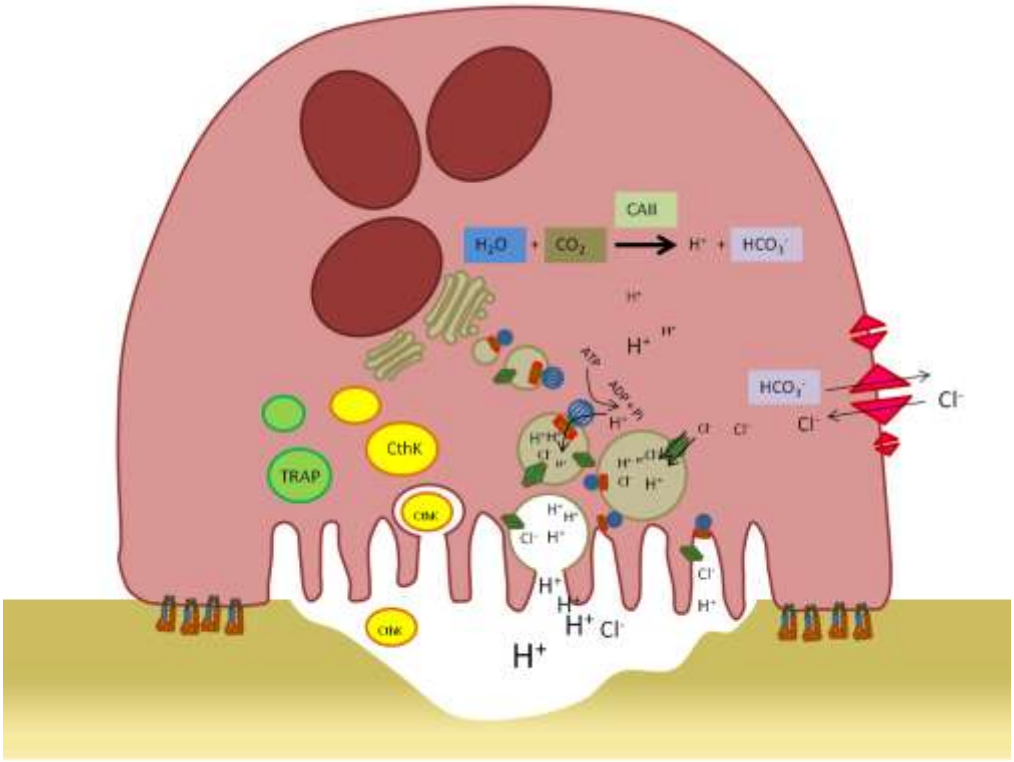

Fig.2 Function of a mature osteoclast and its intracellular activity according to acidification and proteolysis

1.1.6 Regulation of bone remodeling

The adult skeleton is in a dynamic state in which the bone is alternately broken down and reformed by the cooperation of bone cells; osteoclasts, osteoblasts, and osteocytes. This turnover is also called bone remodeling. It is estimated that the remodeling occurs in every 3-4 months in humans[63]. The remodeling initiates with the activation of resorptive activity of osteoclasts. Under physiological conditions, osteoclast precursors are induced by monocyte chemoattractant protein-1 (MCP-1), which can be released by osteoblasts[64], to migrate to the resorption site. The resorption site also provides bone-overlying osteoblasts with RANKL, the paracrine inducing osteoclastogenesis. The cell-cell contact and signals from adjacent bone lining cells permit the nascent osteoclasts to occupy the bone.

As TGFβ and BMPs are embedded in bone during bone formation, when the osteoblasts degrade the bone matrix, these factors are released into the paracellular environment. The rising level of the factors can stimulate the differentiation of the osteoblast precursors to premature osteoblasts. Furthermore, the osteoclasts communicate with osteoblast precursor cells through Eph tyrosine kinase receptor/ligand. EphrinB2 ligand is on the osteoclast membrane and can suppress osteoclast differentiation by blocking the expression of the transcription factor c-FOS. On the other side, Eph receptor EphB4 located on the osteoblast membrane mediates RhoA activity. The activation of EphB4 inhibits the activity of RhoA leading to enhanced osteoblast differentiation in mice [65]. But in humans, it has been found that inhibition of RhoA has the converse function of suppressing the osteoblast differentiation [66]. The bidirectional signaling has been suggested to facilitate the transition from the resorption phase to formation phase [65, 67].

1.2 Osteoclast-associated diseases

Osteopetrosis is a hereditary bone disease resulting from a loss of osteoclast function. Human osteopetroses can be classified by inheritance pattern into autosomal recessive osteopetrosis (ARO) and autosomal dominant osteopetrosis (ADO). According to severity, ARO is divided into two subtypes: malignant infantile type and intermediate type. Malignant ARO (MIM 259700) is more

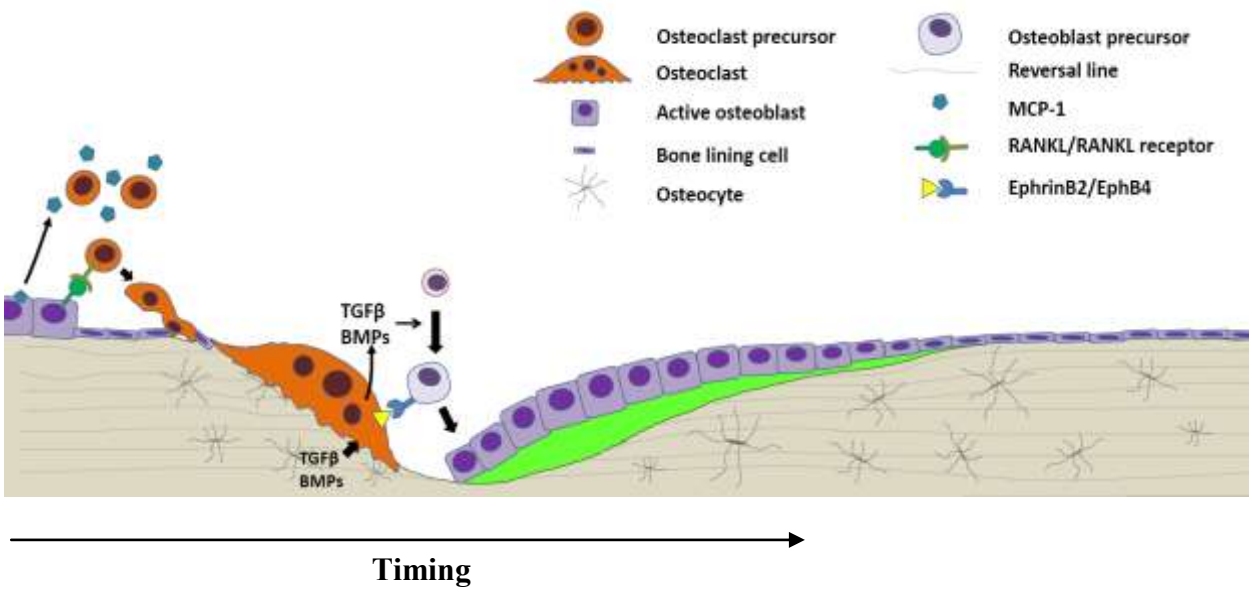

Fig.3 A drawing illustrating the coupling of osteoblasts and osteoclasts for bone remodeling.

severe and can already be detected shortly after birth. This form is uncommon with an average incidence of 1:200,000 to 1:300,000. At present, there are three genes involved in the etiology of malignant ARO. Mutations on *TCIRG1* gene are identified in 50% ARO patients, whereas mutations in *CLCN7* and *OSTM1* gene have been reported in approx. 15% [34, 68-76].

The other recessive form of osteopetrosis is intermediate ARO (MIM 259710). Incidence of this type is very rare. Patients have less severe symptoms with a later onset. The homozygous mutations in *CLCN7* have been reported in this subtype [77]. In addition, autosomal recessive osteopetrosis with renal tubular acidosis (RTA, or aka Guibaud-Vainsel syndrome or marble brain disease; MIM 259730) is an additional form of osteopetrosis. This form has been shown to be caused by homozygous mutations in *CA II* [73, 78].

The autosomal dominant forms of osteopetrosis (ADO) have a relatively benign phenotype with later onset. The frequency of ADO has been estimated to be 1:500,000 to 1:100,000. The patients have milder symptoms that do not reduce life expectancy. Frequently, the diagnosis of ADO is made coincidentally when radiographic investigations are performed for other indications. Subforms of ADO are classified by appearances and severities of sclerotic bone. In the literature [79] it was suggested that at least 3 subforms of ADO have been reported: ADO type I (MIM 607634), ADO type II (MIM 166600), and ADO type III.

ADO type I presents radiographically with generalized, diffuse osteosclerosis, prominent in the cranial vault. To date, ADO I is the only type of osteopetrosis which has been supposed to be a consequence of hyperfunction of osteoblasts. Gain-of-function mutations of a low-density lipoprotein receptor-related protein 5 (LRP5) gene have been identified in ADO type I patients [80, 81].

The first recognized ADO subtype is ADO type II which was described as early as 1904 by Albers-Schönberg, a radiologist from Hamburg [82]. The disease has a reduced penetrance. The symptoms of this subtype are also relatively benign, though they are frequently exposed by their complications, mostly long bone fractures (78%) with or without coinciding trauma [83]. ADO type II manifests radiographically with a particular osteosclerosis, predominantly at vertebral end plate (so called "rugger jersey spine"), periphery of long bone, and skull base. A "bone within bone" sign is mostly restricted to the pelvis [83]. Levels of total acid phosphatases are raised in ADO type II, but not in type I [84]. Iliac crest biopsies in ADO type II revealed an increased eroded bone surface, which indicates elevation of osteoclast number [85]. Accordingly it has been implied that the etiology might be associated with an osteoclast function rather than a defect of osteoclastogenesis. Recently, 55% to 70% of ADO type II have been associated with heterozygous mutations in *CLCN7* [86, 87]. The function of osteoclasts taken from ADO type II in vitro was around 30% of normal control and around 4-fold higher than ARO osteoclasts. A mouse model for the detailed analysis of ADO II is missing.

Alongside ADO I and ADO II, which has main skeletal phenotype at axial bone, ADO III have been reported that the sclerosis dominantly presented at distal and appendicular bone without a "rugger-jersey" spine. This subtype is very rare and its associated gene is still unknown [88].

1.3 Chloride channel 7: a membrane protein related with bone resorptive activities of osteoclast

Voltage-gated CLC chloride channels are a well-conserved family that is structurally unrelated to other known voltage-gated channels. They are found from bacteria to animals. Their functions in higher animals probably include the regulation of cell volume, control of electrical excitability and trans-epithelial transport. The structure of these chloride channels consists of two identical subunits which fold symmetrically. Each subunit has its own high affinity site allowing to bind Cl^- . In eukaryotes, ClCs constitute a family of 9 members including; ClC-1, ClC-2, ClC-Ka,

ClC-Kb, ClC-3, ClC-4, ClC-5, ClC-6, and ClC-7. ClC-1, ClC-2, ClC-Ka, and ClC-Kb exclusively locate to the plasma membrane, while the other ClCs are found in intracellular compartments (Table 1).

ClC-7 is encoded by the *CLCN7* gene which locates on chromosome 16p13. ClC-7 is expressed ubiquitously, but with highest levels in kidney, liver, heart, dorsal root ganglion, trigeminal ganglion, frontal brain, and eye [69]. *Clcn7* KO mice show reduced bone growth and do not survive for more than 6-7 weeks. Histologic findings of tibiae revealed overwhelming bone and osteosclerosis obstructing the bone marrow cavity resulting in a so called “bone within bone” appearance, with no cortex formation. Bone density in secondary spongiosa was raised 6 to 8-fold higher than their littermates. In vitro resorption assays demonstrated that loss of *Clcn7* abolishes osteoclast resorption. Additionally, the mutant mice demonstrated retina and CNS degeneration. Visual loss in osteopetrosis has been mainly attributed to optic nerve compression. However, the visual impairment in osteopetrosis is known to worsen in a subset of patients even after successful bone marrow transplantation [89]. In mice there are clear indications that photoreceptor cells are directly damaged by loss of ClC-7 [90].

Table 1 ClC subfamilies, their cells or organ expressions, their functions, and their relevant conditions or diseases

Position	ClC member	Main site of expression	Functions	Relevant conditions/diseases	
				Mouse model	Human
Plasma membrane	ClC-1	Skeletal muscle	Stabilization of membrane potential	Myotonia (*adr* mouse)	Myotonia congenita
	ClC-2	Broad	Transepithelial or Transplasma membrane pH and volume regulation	Degeneration of retina/testis	Epilepsy (?)
	ClC-Ka	Kidney, inner ear	Transepithelial transport	Diabetes insipidus (renal water loss)	
	ClC-Kb	Kidney, inner ear	Transepithelial transport		Bartter syndrome III (renal salt loss)
Intracellular membrane	ClC-3	Broad	Acidification of endosomes and synaptic vesicles	Degeneration of renal or hippocampus	
	ClC-4	Broad	Unknown		
	ClC-5	Kidney, intestine	Acidification of endosomes	Defect in renal endocytosis	Dent's disease (proteinuria, kidney stones)
	ClC-6	Broad	Unknown		
	ClC-7	Broad	Acidification of lysosomes Balance electric potential of osteoclasts	Osteopetrosis, CNS & retinal degeneration	Osteopetrosis

1.4 Aims of the study

After gaining molecular understanding of pathogenesis of disease, gene replacement therapy is trialed in both animal models and clinical studies. Throughout an improvement of in vitro manipulation of bone marrow stem cells, single gene disorders, e.g. cystic fibrosis and severe combined immunodeficiency (SCID) have been demonstrated a successful of allogeneic haematopoietic stem cell transplantation (HSCT) targeted gene therapy. Likewise, *TCIRG1* as well as *CLCN7* mutations cause ARO. $OC^{-/-}$mice which lack of *tcirg1* homolog can be rescued by *in utero* HSCT (Frattini 2005) and by intraperitoneal transplantation using HSC or fetal liver cells (Johansson 2006, 2007). Beside *tcirg1*, *clcn7* mutations can cause osteopetrosis in mice.

CLCN7 mutations associate with a cause of two subtypes of osteopetrosis. A heterozygous mutation of *CLCN7* induces a less severe type (ADO), whereas a complete mutation causes a severe type (ARO). ClC-7 structure is dimmers, in which each of two subunits has its own pore. At the pore, it has a high affinity for chloride anion and transports the anion through the lysosomal membrane to maintain neutral electricity during proton release. Thus the heterozygous mutations should be encoded for <25% of the entire protein, statistically. The pathogenesis of the disease remains unclear, because the mutations' carriers do not express phenotype as expected. For this reason, the present study was aimed to investigate the degree of ClC-7 expression in association which function of osteoclasts and the severity of the disease. Accordingly, the understanding of pathogenesis of the diseases would be beneficial to develop a proper treatment of the diseases as well as regressive metabolic bone diseases.

TRAcP is an enzyme which strongly express in osteoclasts. The level of ClC-7 expression and function would be conditional on the expression of TRAcP. Thus, the transgen ClC-7 cDNA under the control of TRAcP promoter would be able to rescue bone resorption in knockout mice. Furthermore, by this intervention, ClC-7 cDNA would be differentially translated for the functional protein. The expression and function of the ClC-7 in osteoclasts could be distinguished and result in dissimilar bone phenotypes.

2. Materials and Methods

2.1 Animal models

Three different transgenic C57BL/6 mouse founders (F1, F3, and F7) with various *Clcn7* genotypes were generated in this work. The $Clcn7^{+/+}$, $Clcn7^{+/-}$, and $Clcn7^{-/-}$ mice were planned to transgene with ClC-7 cDNA under control of TRACP promoter. This way, six various genotypes including $Clcn7^{+/+}$ T+/-, $Clcn7^{+/-}$ T+, $Clcn7^{-/-}$ T+ F1, $Clcn7^{-/-}$ T+ F3, $Clcn7^{-/-}$ T+ F7, and $Clcn7^{-/-}$ T- (KO) were categorized.

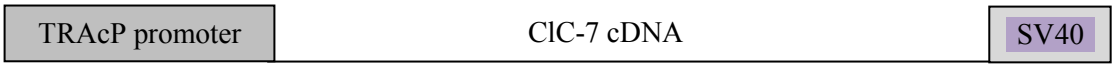

Fig.3 A schematic diagram of transgenic strategy for rescuing osteopetrosis

All mice were of the same lifespan before they were sacrificed.

To investigate a bone turnover rate, 21 mice from F1 and 21 mice of F3 were injected intraperitoneally with 100 μg/g tetracycline on 4 day and 1 day before the day of sample preparation.

2.2 Bone histomorphometric analysis

Bone quality can be measured by many means, i.e. bone mineral density (BMD), micro computerized tomogram (μCT), histomorphometry, as well as x-ray backscattering spectroscopy. Among them, histomorphometry has several advantages such as low budgets, accepted resolution (1-5μm), and uncomplicated approach. Owing to the fact that decalcification process is not required for embedding in plastic, mineralized materials (calcium) in tissues such as bone and teeth can be observed by silver impregnation method (von Kossa's). After reaction by light or chemical agents, the calcium content tissue can be visualized as dark brown or black stain. Von Kossa's method can be counterstained with other dyes such as toluidine blue O, nuclear fast

red, as well as acid light green. The contrast of staining is convenient for further imaging and analysing procedures. Generally, steps in bone histomorphometric analysis are 1) histological process, 2) chemical staining, 3) tissue imaging, and 4) analysing, respectively.

Tibia and femur were selected to be analysed in this study because they have the required amount of bone tissue for investigation. Moreover, their landmarks can be conveniently orientated.

2.2.1 Histological process

After sacrifice, left tibia and femur were fixed in 4% paraformaldehyde in phosphate buffered saline (PBS) at least 24 hours at 4°C. After the fixation, to prevent an adverse effect of paraformaldehyde, the samples were washed several times and kept in PBS at 4°C until histological process. The tibias and femurs were planned to be embedded in methyl methacrylate (MMA) for histomorphometry and paraffin for immunofluorescence, respectively.

2.2.1.1 MMA embedding

Tibias were gradually dehydrated and infiltrated by following steps. All steps were performed at 4°C

- Tissue dehydration in 70%, 80%, 90%, 100%, and 100% ethanol, 24 hours each step
- Clearing with 50% ethanol in acetone for 12 hours
- Reducing the clearing agent with 100% ethanol for 24 hours
- Clearing twice in xylene, 2 hours each
- Embedding material by infiltration twice in infiltration solution, 24 hours each

Next, the samples were embedded in liquid MMA solution and degassed by using an exicator for 10 minutes. Polymerisation of MMA was chemically initiated by DMPT.

2.2.1.2 Paraffin embedding

Protein expression can be detected by enzymatic and immunological methods. Although immunohistochemistry can be done in MMA tissue sections, the results were still not preferred

[91, 92]. Furthermore, in the present exploratory tests in MMA sections, the protein detection (TRAcP staining) was not successful. For that reason, protein preservation in universal paraffin embedding is more reliable than in plastic embedding. Femur is a long bone whose development pattern is very similar to that of the tibia. Hence, to study the in situ expression of the proteins, femurs were chosen. The femurs were decalcified, gradually dehydrated, and infiltrated by following protocol.

- Decalcified twice in 0.25M EDTA in PBS at 4°C for 1 week each step
- Washed out EDTA with PBS several times
- Dehydrated with 60%, 70%, 90%, and 100% isopropanol at 4°C for 2-3 hours each step
- Infiltrated with 50% melted paraffin in isopropanol at 60°C for 12 hours
- Infiltrated twice in melted paraffin for 2-3 hour each step

Finally the samples were embedded in paraffin, and kept at 4°C before sectioning.

2.2.2 Sectioning

2.2.2.1 MMA embedded tibia

Four µm-thick sections were prepared by Leica RM2255 Microtome. For standardization, the series of sections were obtained approximately from 50 µm to 400 µm away from internal surface of lateral cortex. The sections were then placed serially on microscopic glass slide and drenched with stretch solution. After that, the sections were covered with Kisol® film and the excess solution was shed with absorbent paper. To enhance the tissue attachment to glass slide, the sections were pressed and dehydrated in 60°C incubator overnight. For storage, the sections were kept in low humidity until used.

2.2.2.2 Paraffin-embedded femur

Four µm-thick sections were prepared with Microm HM 355 S Microtome and section transfer system. The series of sections were obtained approximately from 50 µm to 300 µm away from posterior surface of internal cortex. The sections were collected on microscopic glass slide and dried in 37°C incubator overnight. The sections were stored in 4°C and low humidified condition.

2.2.3 Embedding material removal and staining methods

2.2.3.1 Deplastination of MMA-embedded tissue

Three sets of 5 slides were collected systematically. The first set was used for dynamic histomorphometry while another two set were used for structural and cellular histomorphometry. Because the fluorescent property of the bone label agent can be bleached during the deplastination process, for dynamic histomorphometry the embedded material was allowed to remain in the tissue. In case of staining, selected slices were soaked in 2-Methoxyethyl acetate (MEA) 3 times each for 10 minutes to remove embedded material. Then the sections were hydrated using descending ethanol concentrations and distilled water. If staining was not urgent, the section was dried at room temperature at least 24 hours or until it was absolute dehydrated.

2.2.3.2 Histochemical staining

For structural histomorphometry purposes, the selected sections were impregnated with silver followed by von Kossa's method and counterstained with toluidine blue O because of high contrast property of the two stainings. Trichrome staining such as Masson-Goldner's, although it is a more complex method, has the advantage that different types of cells can be distinguished easier. Thus, for cellular histomorphometry purposes, the selected sections were impregnated with silver followed by von Kossa method and counterstained using Masson-Goldner's trichrome method.

2.2.4 Histological imaging, measurement and analysis

Histological images used for dynamic and structural histomorphometry were taken with Olympus BX60 microscope and captured by Leica video camera which was controlled by DC Viewer program. Bone morphometry was performed using the KS400 and AxioVision software systems. The measurement was programmed for universal parameters. The nomenclature, symbols, and units of histomorphometry corresponded with the report of the American Society of Bone and Mineral Research Committee (Parfitt 1987).

2.2.4.1 Dynamic histomorphometry

Some fluorochrome can bind to bone tissue during its mineral formation and can be detected under a simple fluorescent light microscope. Hence, this property can be used to observe the rate of bone mineral formation. Tetracycline is safe and may be detected under fluorescent light. For each sample, 10 MMA sections of tibia from 5 slides were selected for mineral apposition rate (MAR) analysis. The apposition rate at anterior and posterior of internal surface of tibia was examined by a distance of two consecutive labels. The labels were defined as two calcein labels which were parallel to each other and present in the area of proximal tibia. Therefore the fluorochrome labeling of bone was captured with 460-490 nm excitation filter using 250x magnification. The lines must be in an upright position at the center of image. The distance between midpoints of parallel lines was directly measured by KS400 software system. MAR was determined by dividing this distance by the labeling period (3 days).

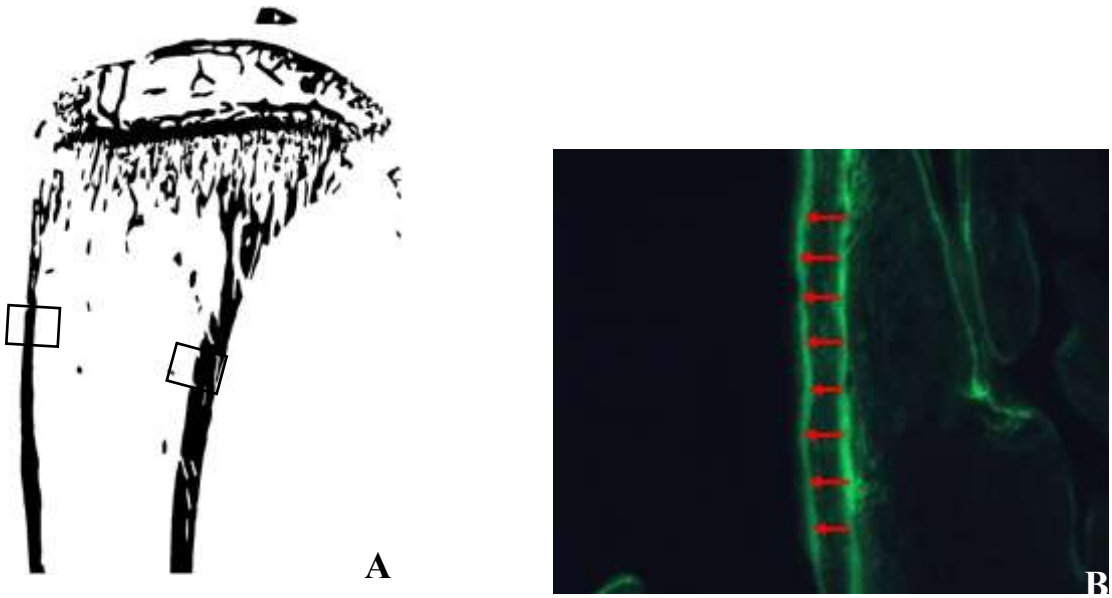

Fig.4 (A) A drawing of sectional tibia depicts two indicative areas of measurement. B) A microscopic image shows a direction (arrows) of bone apposition at internal side of posterior cortex. A distance between these two fluorochrome labels is measured and applied to evaluate mineralized apposition rate (MAR).

2.2.4.2 Structural histomorphometry

For each sample, 15 von Kossa-toluidine blue stained sections of tibia from 5 slides were selected for structural histomorphometry. Images of proximal tibia were taken using 40x magnification.

Growth plate, primary spongiosa, and secondary spongiosa were analyzed by KS400 software to obtain the following bone structure parameters.

The parameters included growth plate thickness, bone volume (B.Ar/T.Ar), trabecular thickness (Tr.Th), trabecular separation (Tr.Sp), and trabecular number (Tr.N). Primary spongiosa histomorphometry was achieved by freehand-making ROI which upper border and lower border are located at lower border of mineralized growth plate and distal end of primary spongiosa, respectively. 0.72 mm^2 quadrate ROI of secondary spongiosa begins at the lower border of primary spongiosa or at a distance of 0.4 mm from the lower border of the growth plate.

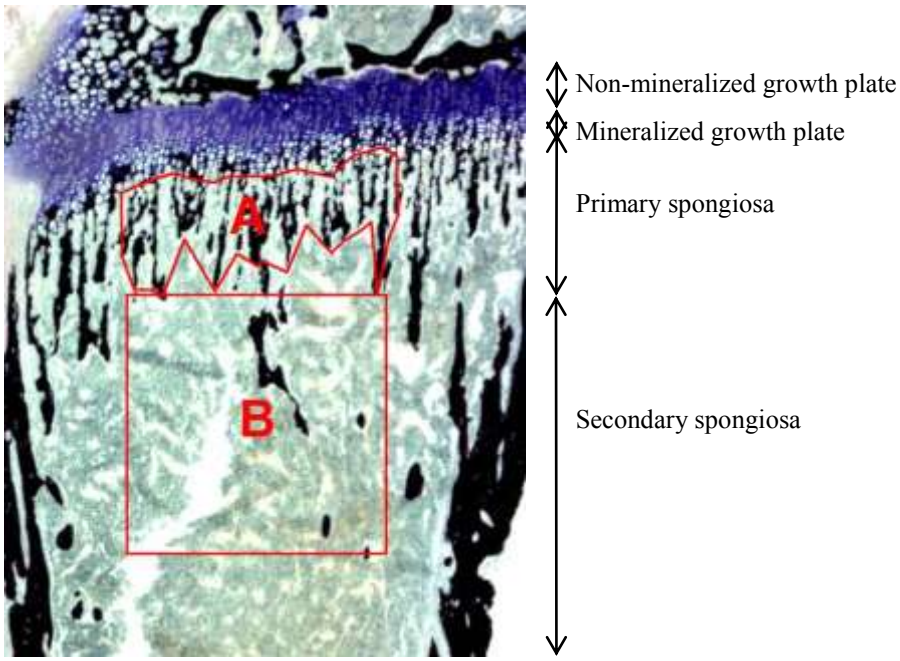

Fig.5 A histological image of proximal tibia is represented with ROI in primary spongiosa area (A) and ROI in secondary spongiosa area (B).

2.2.4.3 Cellular histomorphometry

For each sample, 10 von Kossa with Masson-Goldner's stain sections of tibia from 5 slides were selected for structural histomorphometry. Images of proximal tibia were taken using 200x magnification. Trabecular bone in proximal tibia was examined by two rectangular ROI with similar dimension (0.70x0.25 mm^2). Proximal ROI and distal ROI, were placed respectively at distances of 0.25 mm and 0.50 mm far from growth plate. Both ROIs were located at midpoint of intercortical distance.

Bone cells and osteoid were manually quantified on the basis of the following criteria.

Osteoclast

Inclusion criteria (minimum 2 of these are involved)

1. Concave surface of bone beside cell.
2. Multinuclear cell
3. In the case of proper stained section, cytoplasm stain orange.
4. Cytoplasm is larger than nucleus.

Exclusion criteria

1. Cell shows character of stromal cell or osteoblast.
2. Less than one fourth of cell-bone surface at the bone side contacts the bone (except sealing zone).

Osteoblast

Inclusion criteria (minimum 2 of these are involved)

1. No concave surface of bone beside cell. (This criterion is excepted if osteoid are shown)
2. Cell is cuboidal or polygonal.
3. In the case of properly stained section, cell stains purple.
4. Space between cell and bone is filled by osteoid.

Exclusion criteria

1. Cell shows character of stromal cell or osteoclast.
2. Cell does not contact bone.
3. More than one half of cell is engulfed in mineralized bone.

Osteoid

Inclusion criteria (minimum 2 of these are involved)

1. Matrix stain in green colour. (In case of poor staining, it may show orange.)
2. Presence between cell and mineralized matrix (black).

Exclusion criteria

Adjacent cell is osteoclast.

Primary measurements included number of cells, bone-cell contact surface, and osteoid surface. For analysis, several parameters were derived from some primary parameters, they are shown in Table 2

Table 2 The table categorizes histomorphometric parameters involved in this experiment.

Dynamic histomorphometry	Static histomorphometry	
	Structural	Cellular
Mineral apposition rate; (MAR)	Growth plate thickness Bone density; (B.Ar/T.Ar) Trabecular thickness (Tr.Th) Trabecular separation (Tr.Sp) Trabecular number (Tr.N)	Osteoclast surface; (Oc.S/BS) Osteoclast number; (N.Oc/BS) Osteoblast surface; (Ob.S/BS) Osteoblast number; (N.Ob/BS) Osteoid volume; (O.Ar/B.Ar) Osteoid surface; (OS/BS)

A **B**

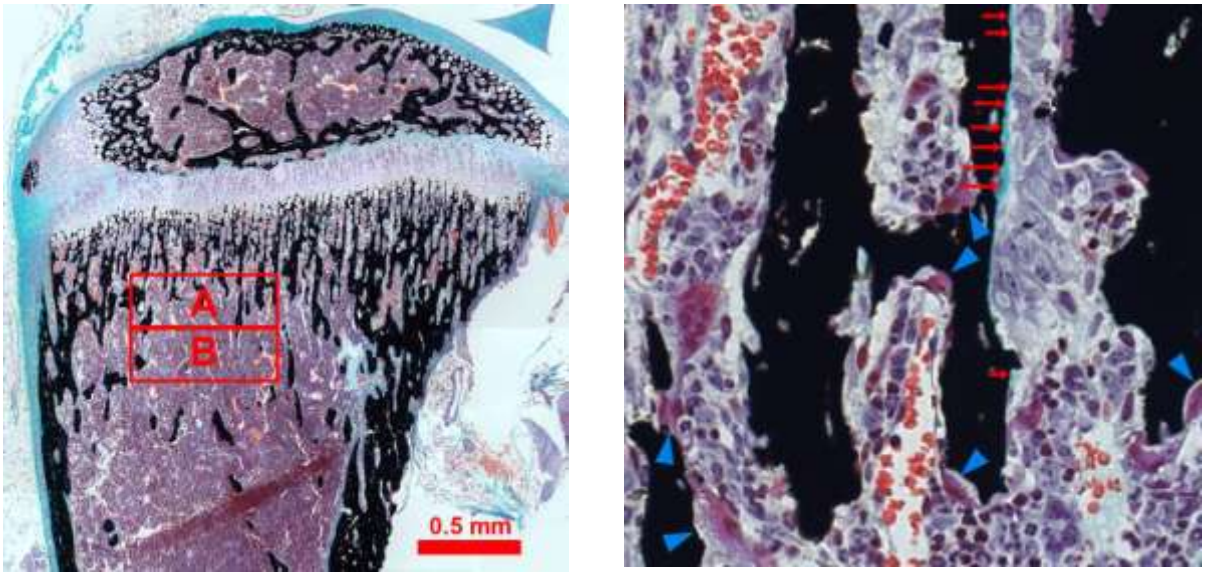

Fig.6 A) The photo image of proximal tibia section stained with von Kossa and Masson-Goldner's staining depicts two representative regions of interest (ROI A and ROI B) located in the secondary spongiosa area. B) Higher magnification (200x magnified) of the same image illustrates black-stained mineralized bone with a high contrast to other structures. Well differentiated multinucleated cells or osteoclasts (arrowhead) lie on mineralized bone surface, resorb it and make a particular concave surface, while cuboidal osteoblasts are seen forming an early new bone or osteoid (stained in light green and pointed by multiple arrows).

2.2.4.4 Statistical analysis

Data are reported as mean ± standard deviation of mean (SD), and standard error of mean (SE). To determine if there were apparent differences in parameters between phenotypes or founders, the variances were analyzed by paired *t-test* or one-way *ANOVA* with differences significant at $P < 0.05$. To determine a correlation of parameters in cellular histomorphometry, they were analyzed by *Spearman* rank coefficient with differences significant at $P < 0.05$.

2.3 In situ expression of osteoclast-related proteins

2.3.1 Sample preparation

Randomized paraffin sections from each group were selected to test expression of proteins by immunofluorescent method. The paraffin sections were deparaffined by xylene and a series of ethanol. An antigen was retrieved in cooked citrate buffer (pH 6.0) heated by microwave for 10 minutes. After slow cooling, the sections were washed 3 times with 0.01% Tween20 in PBS, and then immediately permeabilized and undesired antigen was blocked with 0.1% TritonX100 in 3% BSA in PBS for 60 minutes. Then the sections were incubated at 4°C overnight with the first antibodies which were diluted properly and mixed with a correspondent antibody (the matchings are shown in the Table 3) in 0.05% BSA in PBS. The sections were washed 3 times with washing buffer before being incubated with second antibodies at room temperature for 60 minutes. Finally, they were washed 3 times again and mounted using a thin cover glass and fluorochrome-appropriated adhesive media. The labeled sections were stored at 4°C with light protection until examination.

Table 3 The matching of first antibodies and their compatible second antibodies is shown using their proper dilution.

Section number	First antibodies	Second antibodies
1	Negative control	1:1000 Alexa Fluor® 488 anti-rabbit 1:1000 Alexa Fluor® 555 anti-goat 1:2000 DAPI
2	1:150 rabbit anti-ClC-7 1:200 goat anti-β3-Integrin	1:1000 Alexa Fluor® 488 anti-rabbit 1:1000 Alexa Fluor® 555 anti-goat 1:2000 DAPI
3	1:150 rabbit anti-ClC-7 1:400 guinea pig anti-a3 subunit	1:1000 Alexa Fluor® 488 anti-rabbit 1:1000 Alexa Fluor® 555 anti-guinea pig 1:2000 DAPI
4	Negative control	1:1000 Alexa Fluor® 488 anti-rabbit 1:1000 Alexa Fluor® 555 anti-guinea pig 1:2000 DAPI

Antibody information: rabbit anti ClC-7, guinea anti a3 subunit of V0-ATPase (Thomas Jentsch's Lab; MDC, Berlin), goat anti β3-integrin (Santa Cruz Biotechnology), DAPI (4',6-Diamidino-2-phenylindole, HCl (Santa Cruz Biotechnology)

2.3.2 Detection of fluorochrome-labeled antigens

The fluorochrome signals were detected with a Zeiss 510 META confocal laser scanning microscope (LSM) system. Protocols for the detection including scanning time, pin holes, and filters were adjusted for optimal intensity. All selected sections were examined using the same protocol at 60x magnification. Osteoclasts, as a target of detection, were captured from the areas of high turnover rate of bone, namely at a junction of primary and secondary spongiosa, and inner surface of metaphyseal cortex.

2.3.3 Evaluation of protein expression

The expressions of protein represented by intensity of fluorochrome were compared descriptively by two independent examiners.

2.4 Osteoclastogenesis *in vitro* study

Gene mRNAs and proteins can be extracted directly from interesting tissue, but due to cells and tissue heterogeneity the expression level of the mRNA and protein can be easily mistaken. Bone is composed of a high proportion of extracellular matrix and ground substances. Seeing that chloride channel is highly expressed in osteoclasts which are relatively not overwhelming in bone, the expression of mRNA and protein could not be reliable. Therefore, primary cell culture was selected for studying the expression of the chloride channel in the rescue osteoclasts.

2.4.1 Isolation of osteoclast precursors and generation of osteoclasts

Four long bones of tibiae and femurs and a spleen were surgically removed from a recently sacrificed mouse using CO_2 asphyxiation. The specimens were immediately collected into sterile PBS on ice. Soft tissue around the long bones was gently removed to provide visibility of bone texture. Both ends of the long bones were snipped to expose bone marrow cavity. Bone marrow cells were then flushed out several times with PBS using 27-gauge needle and syringe. Next, spleen was minced in 1 ml PBS on sterile tissue culture dish by using a sterile #10 blade scalpel. The bone marrow cell and spleen cell suspension was passed through sterile 20 μm cell filter into a sterile 50 ml centrifuge tube. The cells were pelletized by centrifugation at 1,000 g for 5

minutes. After that, the supernatant was gently removed. The sediment cells were resuspended with 8 ml 1% penicillin/streptomycin, 10% fetal calf serum (Gibco® Lot.41Q4556K) in αMEM (Lonza, Biowhittaker™) supplemented with 35 ng/ml M-CSF (Peprotech®) and then placed on a ø100 mm sterile bacteria culture plate. The cells were incubated at 37°C with 5% CO^2 for 7 days, and the medium was refreshed every 3 days.

At day 7, non-adherent cells and supernatant were disposed. The remaining adherent cells (or osteoclast precursors) were detached by using 0.5 mM EDTA and then transferred to a 50 ml centrifuge tube. The precursor cells were pelletized by centrifugation at 1,000 g for 5 minutes. The supernatant was gently removed. The sediment cells were resuspended with cell culture medium. Afterwards, cell culture medium supplemented with 25 ng/ml M-CSF and 30 ng/ml RANKL (Peprotech®) was adjusted to maintain cell density at 5 x 10^6 cells/ml. Then 160 µl, 0.8 ml, and 2 ml of the cell suspension were seeded in two 8-well, a 2-well cell culture chambers (Lab-Tek™ II Chamber Slide™), and two ø35 mm cell culture petri dishes (Corning®), respectively. The precursor cells were allowed to incubate at 37°C under 5% CO^2 for 6 days for osteoclast differentiation. Fresh cell culture medium containing 25 ng/ml M-CSF and 35 ng/ml RANKL was renewed every 3 days.

2.4.2 *Clcn7* mRNA expression

2.4.2.1 Cells lysation

The 2-week *in vitro* M-CSF, RANKL-induced osteoclasts cultured in 2-well cell culture chambers and a ø35 mm cell culture petri dish were lysated 5 minutes at room temperature with 0.3, and 0.8 ml TRIzol® reagent, respectively. The lysates were collected in a 2 ml microcentrifuge tube and stored at -20°C.

2.4.2.2 RNA isolation

The lysates were centrifuged at 4°C at maximum speed for 5 minutes. 1000 µl supernatant was transferred into new RNAse-free 1.5 ml microcentrifuge tubes containing 200 µl chloroform. The solution was vigorously shaken for 15 seconds, and left at RT for 15 minutes. The mixtures were centrifuged at 12,000 rpm at 4°C for 15 minutes. The upper most phase containing rich RNA was then transferred into new 1.5 ml microcentrifuge tubes. 500 µl Isopropanol was added

into each tube. The mixtures were left to incubate at RT for 10 minutes prior to centrifugation at 12,000 rpm for 15 minutes at 4°C. Supernatants of each tube were carefully removed. The pellets were cleaned by adding 500 µl RNAse-free 70% ethanol and then mixed using a vibrator. The mixtures were centrifuged at 12,000 rpm at 4°C for 15 minutes. Supernatants of each tube were carefully removed. The pellets were cleaned again by adding 500 µl RNAse-free 100% ethanol and mixed vigorously using a vibrator. The mixtures were centrifuged at 12,000 rpm at 4°C for 15 minutes. Supernatants of each tube were carefully removed. The pellets were immediately dried in a speed vac for up to 10 minutes. The pellets were dissolved in 100 µl DEPC H_2O. The RNAs were cleaned up, and decontaminated DNAs were digested in column according to the instruction of Qiagen® RNeasy mini kit. The purified RNAs were stored at -80°C

2.4.2.3 RNA quality check

The purified RNAs were checked for concentration at 260 nm and 280 nm photometrically. An appropriate quantity of DEPC H_2O was added to become accustomed the concentration to 25 ng/µl. The 0.25 µg RNAs diluted with DEPC H_2O and gel-loading buffer were loaded on a 1.5% fresh agarose gel for checking 18S RNA and 28S RNA.

2.4.2.4 First-strand cDNA synthesis

After the quality check, to anneal RNAs, primer/RNAs mix (12 µl) was prepared as follows. The RNA mix was heated at 65°C for 5 minutes to denature secondary structures of RNAs and then suddenly chilled on ice. A mastermix was prepared and added to the denatured primer/RNAs mix.

Primer/RNAs mix:		Mastermix:
10 µl	RNA (250 ng)	4 µl 5X first-strand buffer
1 µl	random primers	2 µl 0.1 M DTT
1 µl	dNTP Mix	1 µl ribonuclease inhibitor (RNaseOut™)

The contents of the tube were mixed gently and incubated at 25°C for 2 minutes before adding 1 µl reverse transcriptase (SuperScript™ II RT). Negative control of cDNAs was constructed without the addition of reverse transcriptase. The first-strand cDNAs synthesis was performed by incubating at 25°C for 10 minutes, 42°C for 50 minutes, and 42°C for 15 minutes subsequently.

2.4.2.5 Quantitation of RNAs expression by quantitative RT-PCR

Quantitative RT-PCR provides an accurate method to determine levels of specific DNA and RNA in tissue samples. It is based on detection of a fluorescent signal produced proportionally during amplification of PCR product.

20 µl first-strand cDNA was diluted with 20 µl H_2O. For each sample, cDNA was set for two PCRs. Next, three random samples were selected for different dilution as cDNA concentration controls (1:3, 1:9, and 1:27). For each PCR, 3 µl cDNA mixtures was pipetted into a 384-well PCR plate (Applied Biosystems) presenting with the premix containing 5 µl of 125 nM of primers (listed in the following table) and 8 µl SYBR-Green PCR Master Mix (Applied Biosystems). The PCR was run on ABI Prism 7700 Sequence Detection System. Thermal cycling conditions were as follows:

Table 4 Thermal cycling conditions used for amplification of cDNA

	Step	Temperature	Time	
1.	Annealing	50°C	2 min	
2.	Denaturing	95°C	10 min	
3.	Denaturing	95°C	15 sec	repeated 45 cycles
4.	Extension	60°C	1 min	
5.	Storage	4°C	forever	

Table 5 List of investigated gene mRNAs and primers

Gene	Forward primer	Reverse primer	note
Gapdh	AGCCTCGTCCCGTAGACAAAA	TGGCAACAATCTCCACTTTGC	
Ctsk	GCTGTGGAGGCGGCTATATG	AGAGTCAATGCCTCCGTTCTG	
Trap	TCCTCGGAGAAAATGCATCAT	GCAGTTAAGCTCCTGGACCAA	
Clcn7	CGGCTTTCCGGACAGTGG	CACGGATCCTGAGTGGAT	primer 6
Clcn7	ATGAACAACGTGGAGCTGGATGA	TTGTCATAGTCCAGGCTCTCATAC	primer 8

Data were collected and analyzed with the Sequence Detection System; SDS 2.1 software (Applied Biosystems). The analysis of gene RNA expression was performed using the two step comparative C_T method. By the first comparative C_T (ΔC_T), C_T of gene RNA was compared to C_T of an endogenous control, glyceraldehyde-3-phosphate dehydrogenase (Gapdh). The second comparative C_T ($\Delta\Delta C_T$), ΔC_T of samples of experiment groups i.e. Het, F1, and F3 were compared to average ΔC_T of sample in Ctl group.

2.4.3 ClC-7 expression of osteoclast *in vitro*

The cells cultured on 35 mm cell culture dish were washed quickly with PBS, and then lysed with 150 µl 1% Triton X100. The contents were employed for ClC-7 expression by Western blot.

2.4.4 *In vitro* osteoclast quantification

2.4.4.1 Fixation and osteoclast staining

Cells in 8-well Labtek were fixed with 4% PFA in PBS at 4°C for 10 minutes. The cells were then washed two times with PBS. After that, the cells in each well were incubated in 1 ml TRAcP staining solution at 37°C for 45 minutes. The cells were washed 3 times with PBS before being incubated in the mixture of 1:1000 DAPI, 1:500 Alexa Fluor® 488 phalloidine in 3% BSA

in PBS at room temperature for 60 minutes. The cells were washed 3 times with PBS before finally being mounted with cover glass.

2.4.4.2 Cells imaging and quantification

Ten ROIs from each sample were selected for osteoclast quantification. Images of the cells were taken with Olympus BX60 microscope and captured with Zeiss video camera which controlled by the AxioVision software system. Each ROI, three images including nucleus of cells dyed with DAPI, TRAcP staining cells, and F-actin using phalloidine were systematically recorded. All TRAcP image capture controls were set to identical properties i.e. exposure time, contrast, and brightness. The original images were overlayed by using the NIH ImageJ picture analysis program. TRAcP positive cells and multinucleated cells (cell containing two or more nuclei) were counted, and their percentages determined.

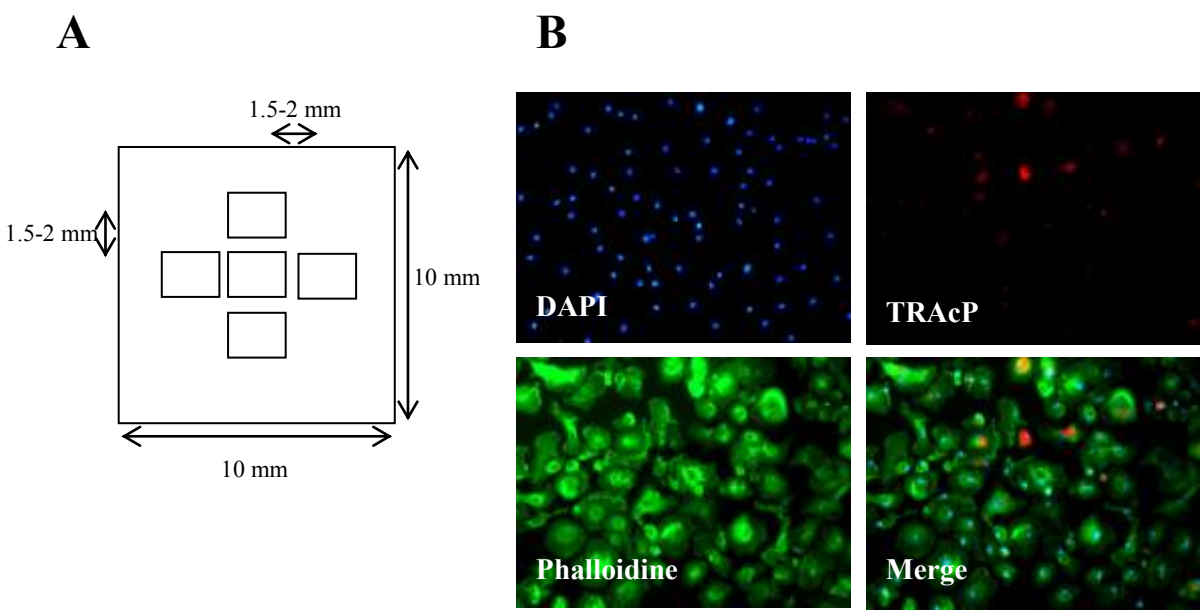

Fig.7 (A) A drawing showing dimensions of an 8-well cell culture chamber, and locations of ROIs in osteoclast quantification. (B) DAPI are used for nucleus determination, TRAcP expression are verified by using a red fluorescent filter, an appropriate image capture setting, and phalloidine staining stands for F-actin which specifically formed in osteoclasts.

3. Results

3.1 Analyzed specimens

Clcn7$^{+/-}$ T+ mice were generated by crossing transgenic (T+) mice from lines F1, F3 and F7 with Clcn7$^{+/-}$ heterozygous knockout mice. All tissue and cell samples used in this study were derived from four-week-old mice from *Clcn7*$^{+/-}$ T+ x *Clcn7*$^{+/-}$ T+ breedings. The resulting mice were classified into six groups according to their genotype (Table 6). As the sex-dependent differences can be neglected at this stage of development male and female specimen were pooled in the same group.

Table 6 Genotype and gender of investigated animals (n.d.* = not defined)

genotype	ClC-7 +/+ T+/-	ClC-7 +/- T+	ClC-7 -/- T+ F1	ClC-7 -/- T+ F3	ClC-7 -/- T+ F7	ClC-7 -/- T-
abbreviation	Ctl	Het	F1	F3	F7	KO
male	12	8	6	8	4	5
female	5	7	10	3	0	0
n.d.*	4	3	1	4	0	0
total	21	18	17	15	4	5

While *Clcn7*-/- T+ mice from lines F1 and F3 had a normal stature, they showed abnormal behaviour which correlated with a neurodegenerative phenotype as previously described by Kasper et al. [93]. *Clcn7*-/- T+ animals from line F7 showed a similar osteopetrotic phenotype as ClC-7-deficient mice (KO), most likely due to absence of expression of the transgenic construct. These animals were therefore excluded from the detailed analysis.

3.2 General morphology

Bone length and overall morphology of Het, F1 and F3 tibiae was comparable to the Ctl group. In contrast, F7 and KO tibiae were shorter, brittle, and lacked marrow cavities. Furthermore, a slight elongation of the hypertrophic zone was observed in the growth plate of KO mice. The primary spongiosa in F1 appeared elongated, and the amount of capillaries at the chondro-osseous junction was reduced. The cortical bone was normally developed in all groups except F7 and KO, in which an abnormally thin, multi-layered cortical bone was formed that corresponds to the bone-within-bone sign in human ARO.

Fig.8 Histologic images of longitudinal sections of tibia reveal different degrees of bone sclerosis. Mineralized bone is stained black, growth plate cartilage and cell nuclei are stained in blue. The sections that were used in structural histomorphometry were stained using the von Kossa method and counterstained with Toluidine blue O.

Unlike long bones, which are formed by endochondral ossification, most parts of the skull are constituted by intramembranous ossification. The skull phenotype in the transgenic mice was assessed by clinical inspection and x-ray images. In KO mice a well vascularized and calvaria with normal thickness were noticed. Transgene expression not only rescued the long bone phenotype, but also tooth eruption. The mice can be fed normal chow. Moreover, as can be seen in Fig.9, the KO skull demonstrates an osteosclerosis at the base, as well as at the cervical vertebrae. Remarkably, incisors, as well as molars are hindered from erupting and a root deformation is observed. Conversely, F1 and F3 skulls demonstrated reversed skull phenotypes, namely normal bone density, tooth eruption, incisor root formation.

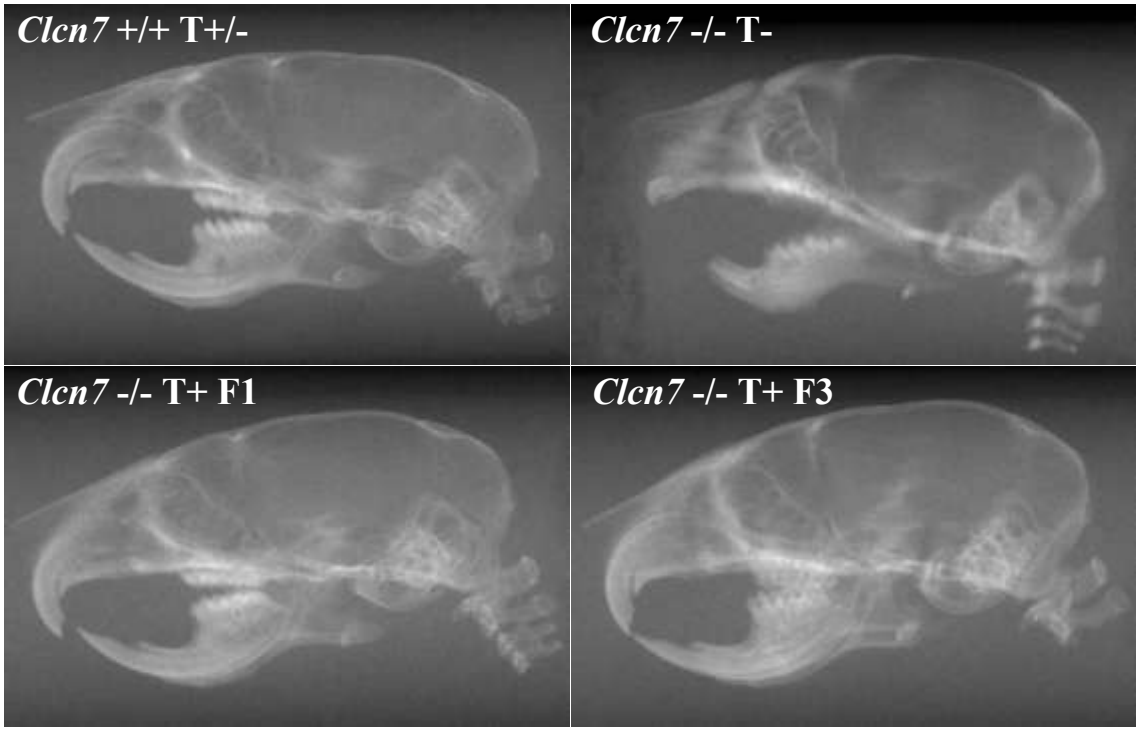

Fig. 9 Radiographic images taken from μCT scout views of 4-week mouse skulls illustrate representative skull phenotypes of Ctl, KO, F1, and F3.

3.3 Histomorphometrical analysis

3.3.1 Static histomorphometry

While the primary spongiosa is formed around the remnants of mineralized cartilage that are not removed in the resorption zone, the secondary spongiosa is the result of the activity of osteoblasts and osteoclasts in the framework of bone remodeling. Therefore, the analysis of both cancellous bone compartments reveals different aspects of bone cell function.

The result of the histomorphometric analysis critically depends on the selection of the respective region of interest (ROI). The ROI for the secondary spongiosa was defined as the region adjacent to the primary spongiosa. In KO and several F1 animals in which the primary spongiosa was massively extended, the upper border of the ROI was placed 400-500 µm distal to the growth plate. Bone density (B.Ar/T.Ar.; %), trabecular thickness (Tb.Th; µm), trabecular separation (Tb.Sp, µm), and trabecular number (Tb.N, mm^{-1}) were the parameters assessed in the histomorphometric analysis. Primary and secondary spongiosa were measured by means of the KS400 software.

3.3.1.1 Thickness of the primary spongiosa

In KO mice a bona fide secondary spongiosa is missing indicating a severe disruption of bone remodeling. Therefore, the measurement of KO primary spongiosa was not possible. The thickness of the primary spongiosa in F1 was significantly increased compared to Ctl, Het, and F3 ($P<0.05$). This effect was less pronounced in F3 tibiae.

3.3.1.2 Growth plate thickness

Growth plate thickness depends a) on the velocity of proliferation and differentiation of the chondrocytes and b) on the resorption of hypertrophic chondrocytes by osteoclasts. The thickness of the growth plate was comparable in all groups, although KO showed a tendency towards an increased growth plate thickness.

3.3.1.3 Bone density

Bone density is a function of trabecular separation and trabecular thickness. Bone density of the primary spongiosa of F1 mice was significantly higher than that of F3, Het, and Ctl (P<0.05). The primary spongiosa bone density of KO mice was also elevated, but the difference to the Ctl was not significant. The secondary spongiosa of KO mice was 6 to 10-fold higher (47.98±7.28%) than F3 (8.49±2.67%), Het (7.449±3.81%) and Ctl (5.87±2.25%), and 3.5-fold higher than F1 (13.02±6.53%). F1 animals had a significantly higher bone density than F3, Het, and Ctl (P<0.05). In contrast, bone density of F3 was only mildly increased. The difference to Ctl (P<0.05), but not to Het mice, was significant.

3.3.1.4 Trabecular thickness

The trabecular thickness reflects the bone forming activity of osteoblasts within the cancellous bone. Average trabecular thickness in the primary spongiosa was not altered in Ctl, Het, F1, and F3 (0.030-0.031 mm), but trabeculae were slightly thinner in the KO group (0.026±0.001 mm, P<0.05). Conversely, secondary spongiosa trabeculae in KO had a slightly increased thickness. Unlike KO, F1 had slightly thicker trabeculae in primary spongiosa, but thinner trabeculae in the secondary spongiosa (P<0.05).

3.3.1.5 Trabecular separation

The average distance between the trabeculae of F1 and KO in the primary spongiosa was significantly smaller (P<0.01 and P<0.05 calculated by F1 and KO respectively). F1 trabecular separation was higher than KO, but was not significantly different from KO. In secondary spongiosa F3, F1, and KO had considerably less trabecular separation than control or heterozygous mice (P<0.01). KO trabecular separation was significantly less than F3 and F1 (P<0.01). Although F1 had relatively lesser spacing than F3, but they were not different statistically.

3.3.1.6 Trabecular number

The parameter trabecular number is a parameter that is generally thought to mirror osteoclast resorptive activity. In the primary spongiosa, F1 and KO had more trabeculae than F3, Het, and Ctl ($P<0.05$). KO mice had more trabeculae than F1, but the difference was not significant. Trabecular number of all groups except KO diminished enormously from around 10 mm^{-1} in primary spongiosa to around 2-3 mm^{-1} in the secondary spongiosa, whereas KO retained high numbers of trabeculae in both zones (from 13.76 mm^{-1} to 9.01 mm^{-1}). In the secondary spongiosa, F3 and F1 had a higher trabecular number than Ctl and Het, but less than KO ($P<0.05$). Moreover, F1 had significantly more trabeculae than F3 ($P<0.05$). This indicates that the impairment of osteoclast activity is KO>>F1>F3.

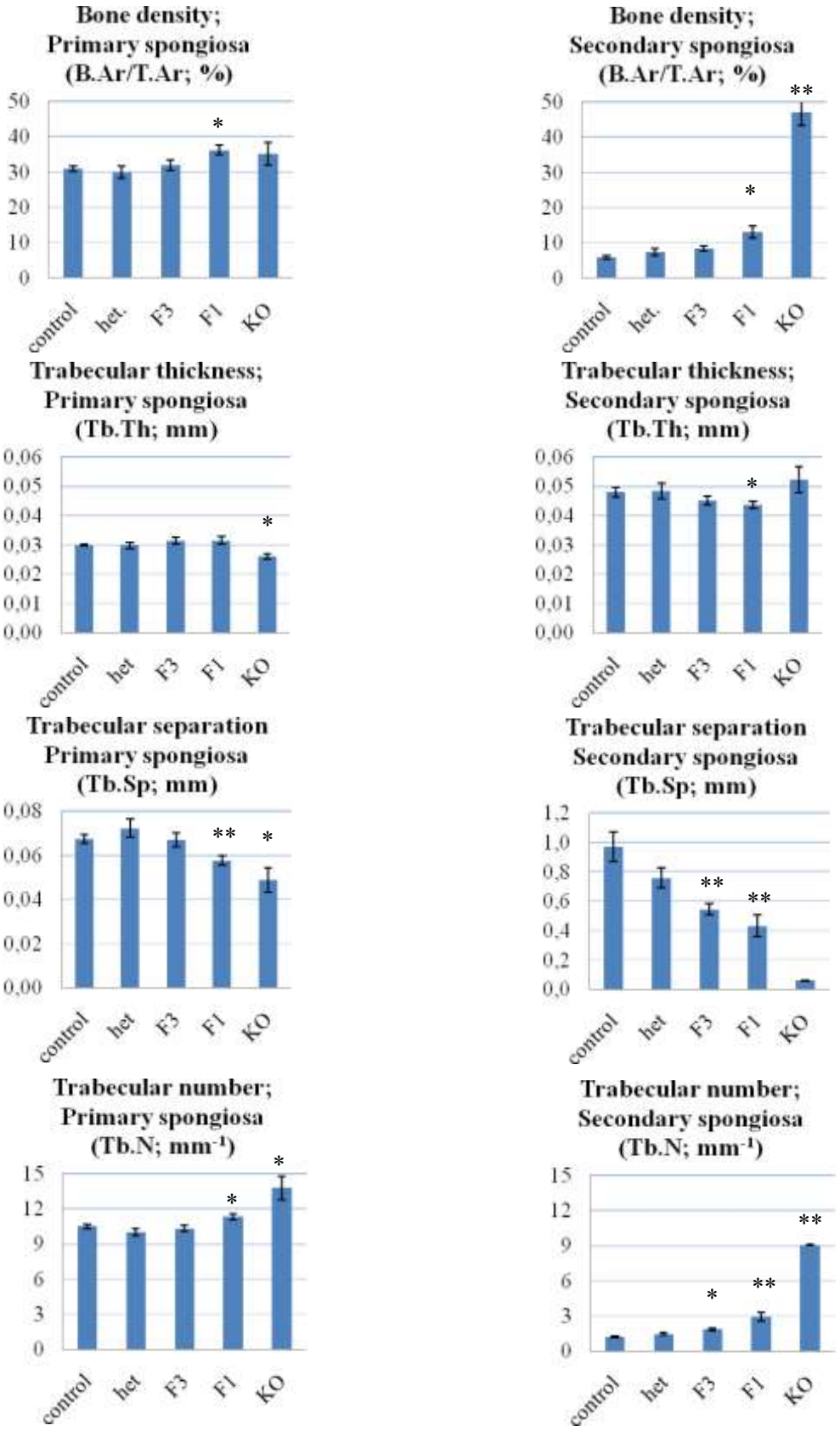

Fig.9 Histomorphometry results in primary spongiosa (left group) and secondary spongiosa (right group). * and ** indicate $P < 0.05$ and $P < 0.01$, respectively.

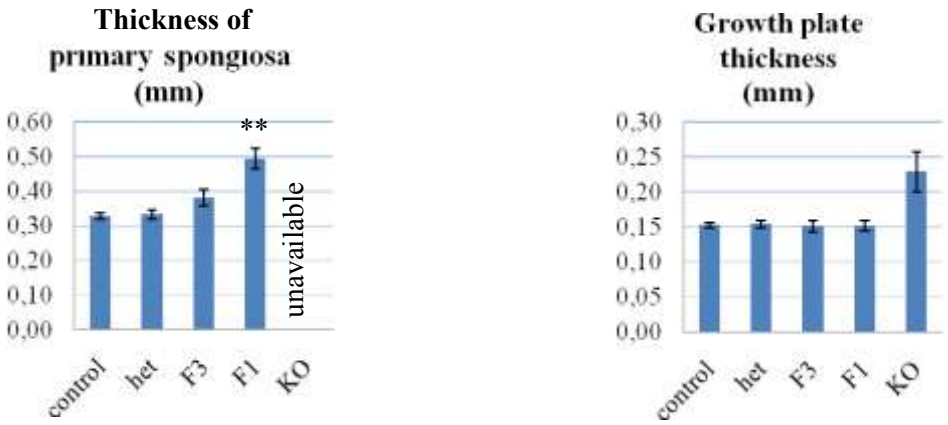

Fig.10 Bar diagrams demonstrate growth plate and primary spongiosa thickness. ** indicates $P < 0.01$.

3.3.2 Dynamic histomorphometry

Fluorochrome labeling of the growing bone allows to assess the rate of bone formation by measuring the distance between two labels. In principle this measurement can be performed in both, the cancellous and the cortical bone compartment, but data collection and reliability are better in the cortical compartment. The results are shown in Table 8 and in Fig.11. Due to the absence of cortical bone KO was not included. The mineral apposition rate at the anterior cortex was similar in all analyzed groups (around 4.3 to 4.5 µm/day). In contrast, bone formation at the posterior side was faster and showed differences. Mineral apposition rate was lowest in F1 animals ($P < 0.05$). Furthermore, the fluorochrome labels in F1 were almost parallel while in the other three groups labels appeared convergent (Fig.12). This indicates a subtle decrease in bone formation in F1 animals.

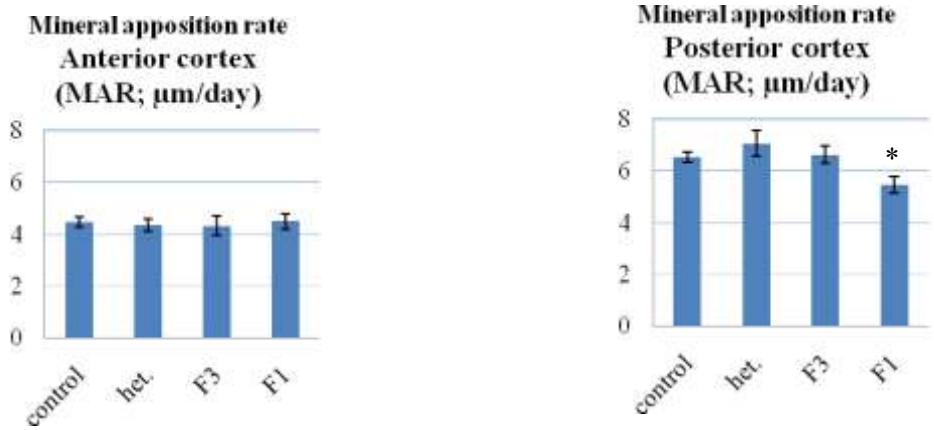

Fig.11 Results of dynamic histomorphometry. * indicates $P < 0.05$.

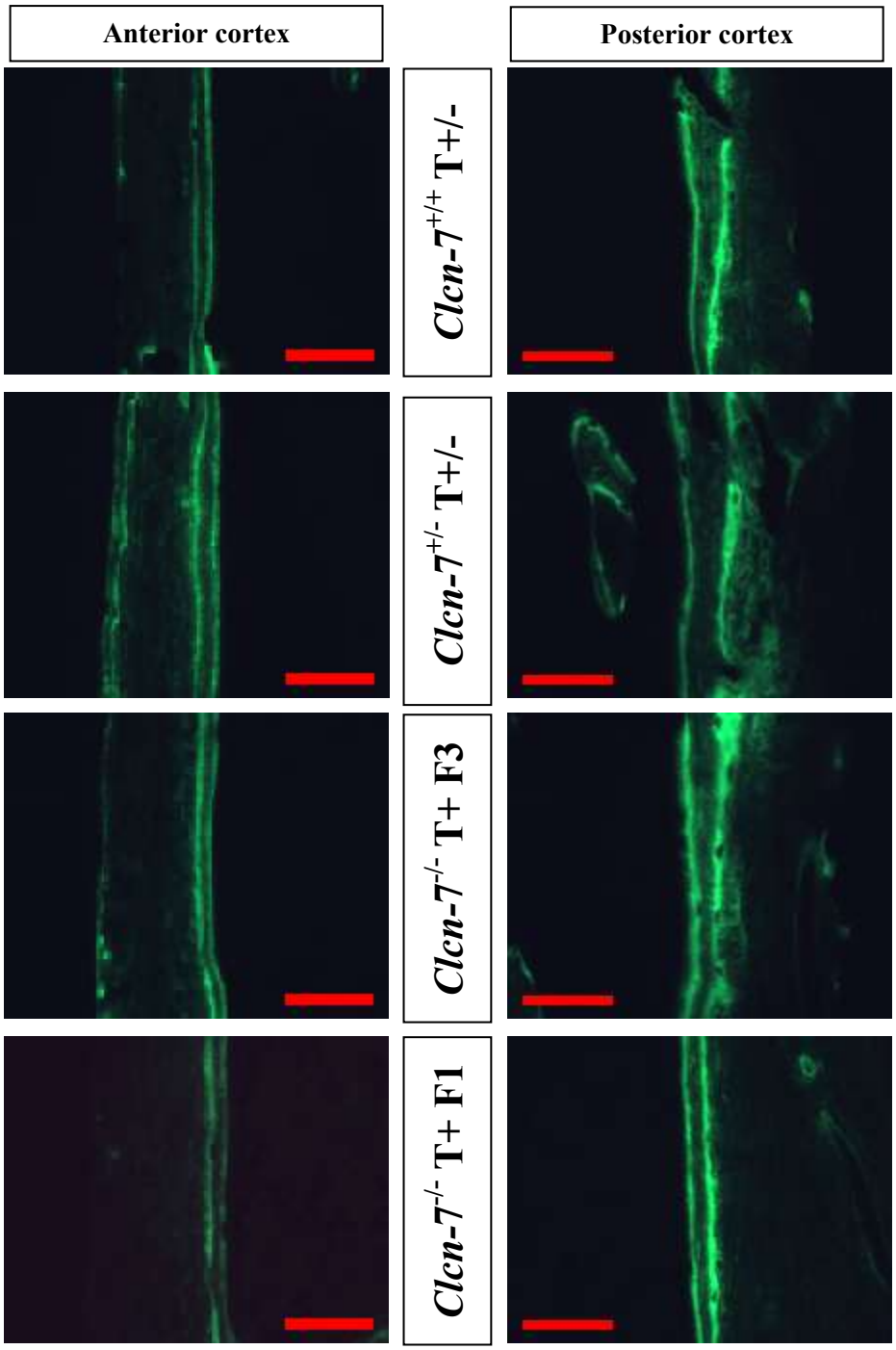

Fig.12 Bone turnover rate at inner surface of anterior (left) and posterior (right) metaphyseal cortex. Scale bar = 100 μm.

3.3.3 Cellular histomorphometry

Two regions of interest were defined for the cellular histomorphometry. ROI A was a region of primary-secondary spongiosa connection, while ROI B purely comprised secondary spongiosa. Quantitative analysis of bone cells including osteoblast number (N.Ob/B.Pm), Osteoclast number (N.Oc/B.Pm), Osteoblast index (N.Ob/Ob.Pm), Osteoclast index (N.Oc/Oc.Pm) and supplemental bone-determinationhave been selected. The results are shown in Fig.13 and Table 9.

2.3.3.1 Osteoblasts and bone formation

The osteoblast number per bone surface was around 15 mm^{-1} in Ctl and Het in ROI A. F3 had slightly less osteoblasts, whereas F1 and KO showed dramatically reduced osteoblast numbers compared to Ctl and Het ($P < 0.01$). Compared to ROI A, there were more osteoblasts in ROI B of all groups, particularly in Ctl and Het. When the numbers were compared among groups in ROI B, F1 and KO had only about 30% of the Ctl osteoblast numbers ($P < 0.01$). The osteoblast index describes the osteoblasts' size. Osteoblast index of F1 was lower than in other groups in both ROIs. From ROI A to ROI B the osteoblast index increased in all groups except KO ($P < 0.01$). Osteoid, newly formed bone by active osteoblast was found predominantly in ROI B of control and heterozygotes and both ROIs of KO. In ROI B, the osteoid volume was enhanced compared to ROI A of the Ctl and Het. In contrast, osteoid was only scarcely formed in both ROIs of F1.

2.3.3.2 Osteoclast

Osteoclast numbers per bone surface were extremely low in KO. Except in F1, osteoclast number increased from ROI A to ROI B. F1 Osteoclast numbers were reduced in ROI A ($P < 0.05$), but showed an marked increase in ROI B to reach nearly the same levels as Ctl and Het. This increase was significantly different from other groups ($P < 0.01$) and most likely reflects an attempt to compensate for the impaired osteoclast activity in F1.

2.3.3.3 Bone density

Bone density was measured additionally, the focus being on mineral part of bone. The highest bone density was found in KO and ROI A of F1. Although F1 bone density declined in ROI B at the same rate as in Ctl and Het, it remained significantly higher ($P < 0.01$).

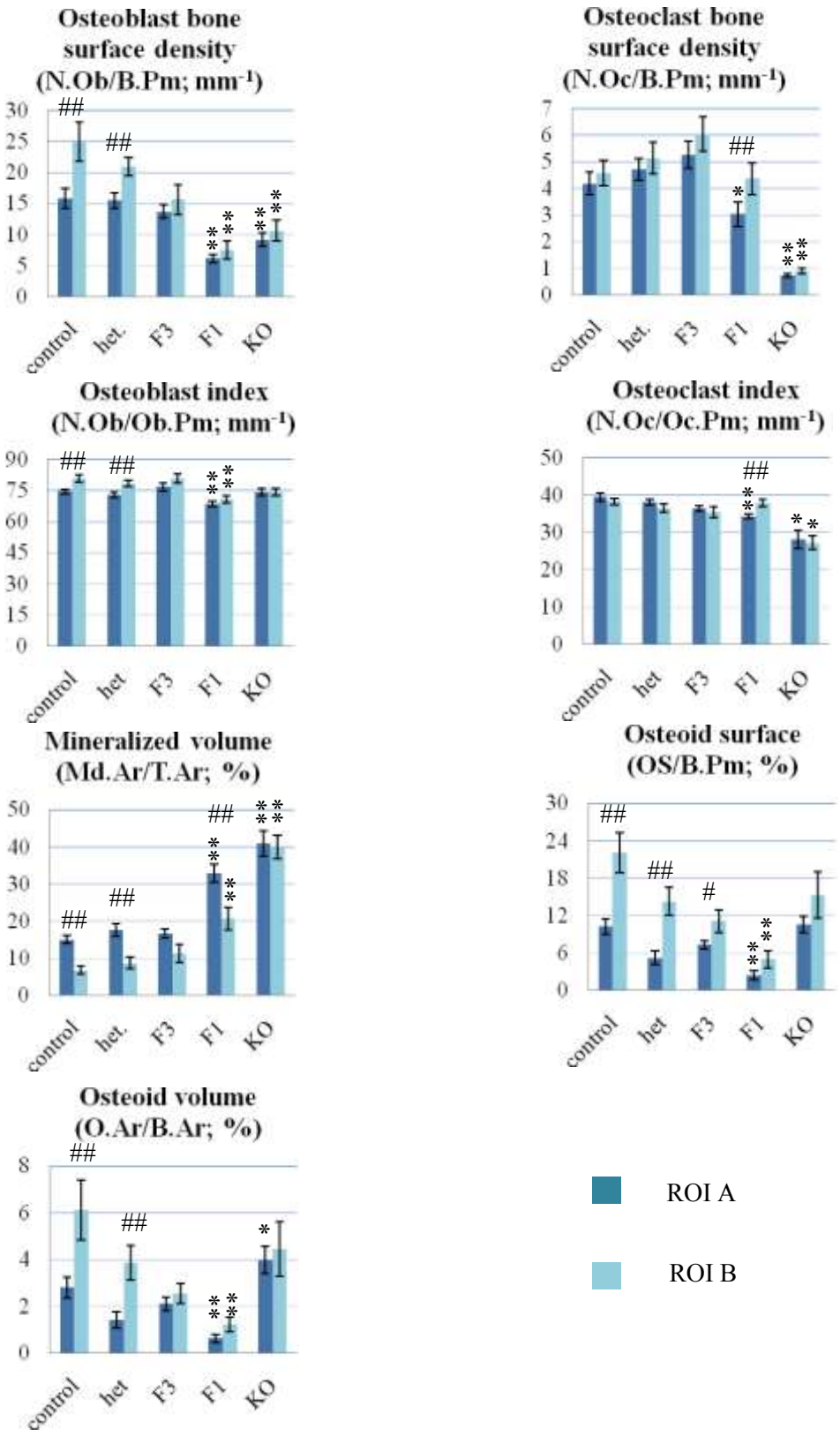

Fig.13 Cellular histomorphometry in ROI A (deep blue bar) and ROI B (pale blue bar). * and ** indicate between group comparison and mean $P < 0.05$ and $P < 0.01$ respectively, whereas # and ## used for ROI A-ROI B comparison and indicate $P < 0.05$ and $P < 0.01$ respectively.

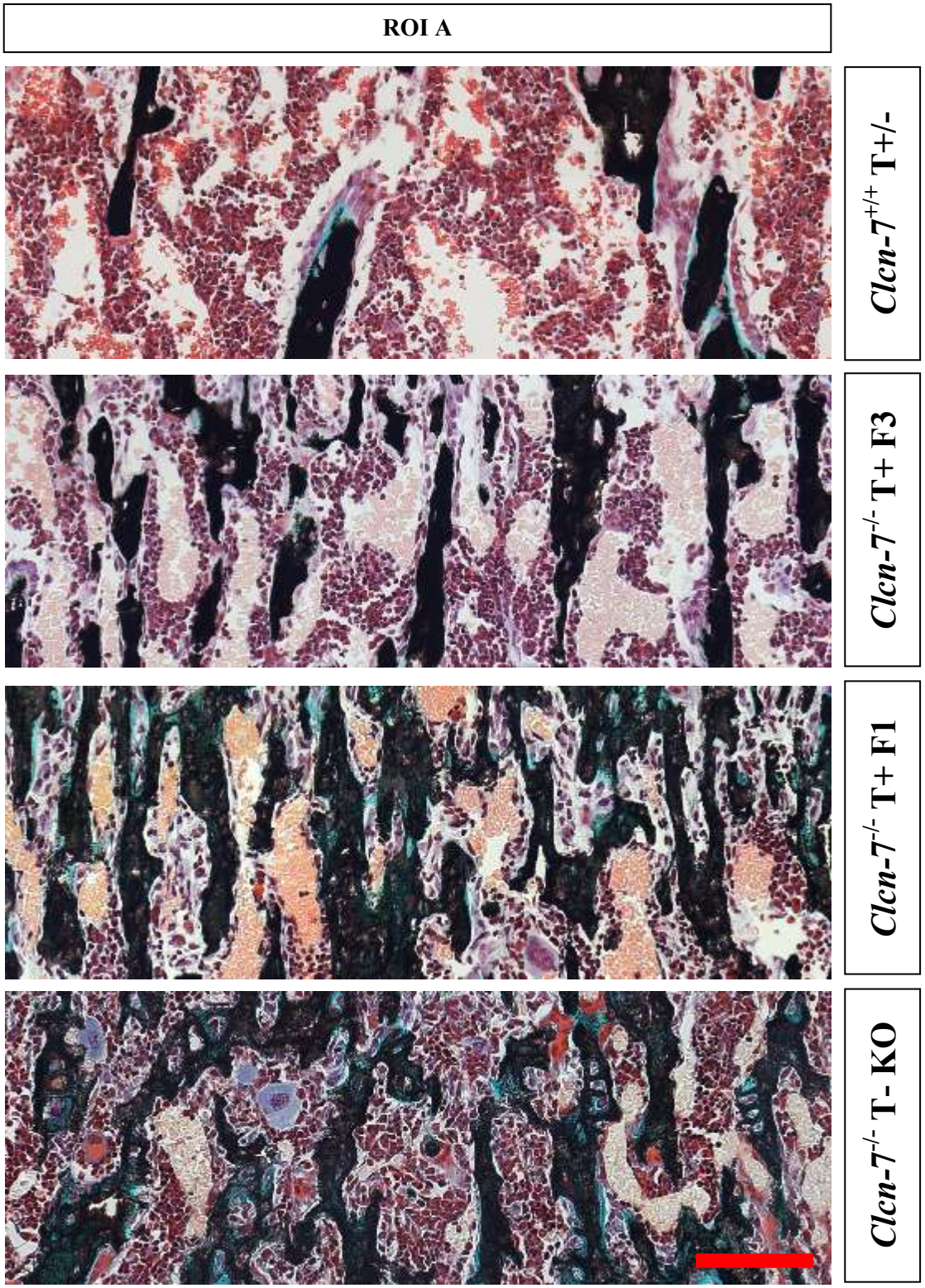

Fig.14 Representative histological images from ROI A of different genotypes (von Kossa with Masson-Goldner's staining, 200x magnification, scale bar = 100 μm)

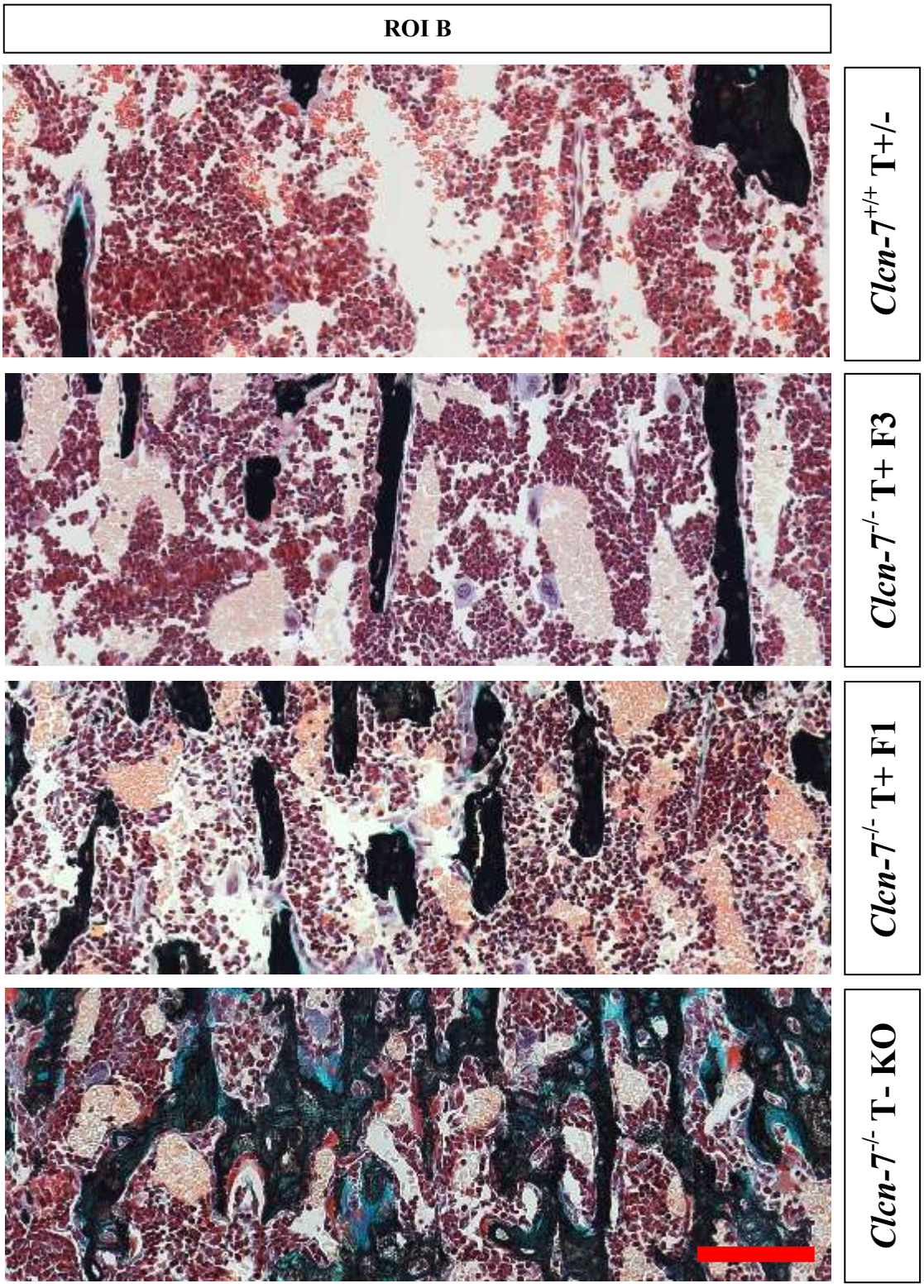

Fig.15 Representative histological images from ROI B of different genotypes (von Kossa with Masson-Goldner's staining, 200x magnification, scale bar = 100 μm)

3.4 Bone cells and bone density relationship

The data from ROI A and ROI B were pooled, recalculated, and demonstrated in line graphs as shown in figure R9. A few F3 specimens reached a cancellous bone density of up to 20%, whereas 9 from 13 F1 tibiae show bone densities from 20% up to 45%. There was no remarkable relationship between bone density and bone cell numbers in Ctl, Het, and F3. In contrast, in F1 osteoblast and osteoclast cell counts seemed inversely correlated to bone density.

Therefore data of bone density and cells quantity from all groups except KO were analyzed. Three scatter plot graphs were generated to exhibit correlations of bone density-osteoblast number, bone density-osteoclast number, and osteoblast number-osteoclast number (figure R10). When bone density increased osteoblast numbers were reduced with an intermediate correlation (r=-0.647). The same tendency was observed for osteoclasts (r=-0.540). Osteoclast number was associated with osteoblast number with a weak correlation (r=-0.504). However, from significant test of correlation, the three correlations were accepted with p<0.001. Notably, no correlation of bone density and quantity of the cells was observed at bone densities below 20%. This means that the correlation is mostly based on the F1 animals.

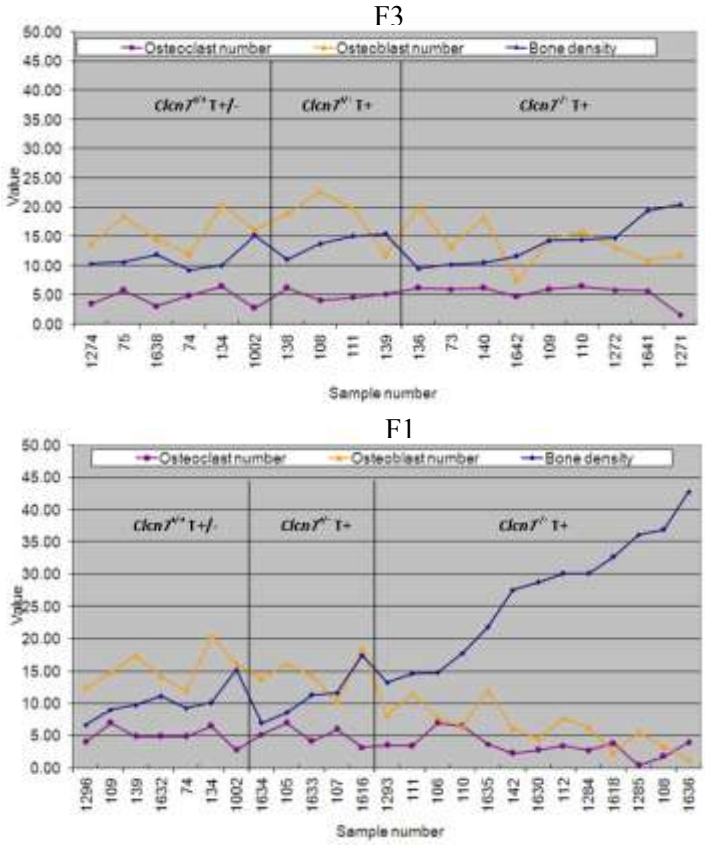

Fig.16 A line graph of bone density, osteoclast number and osteoblast number in F3 (above) and F1 (below). The sample numbers are arranged by genotype and bone density.

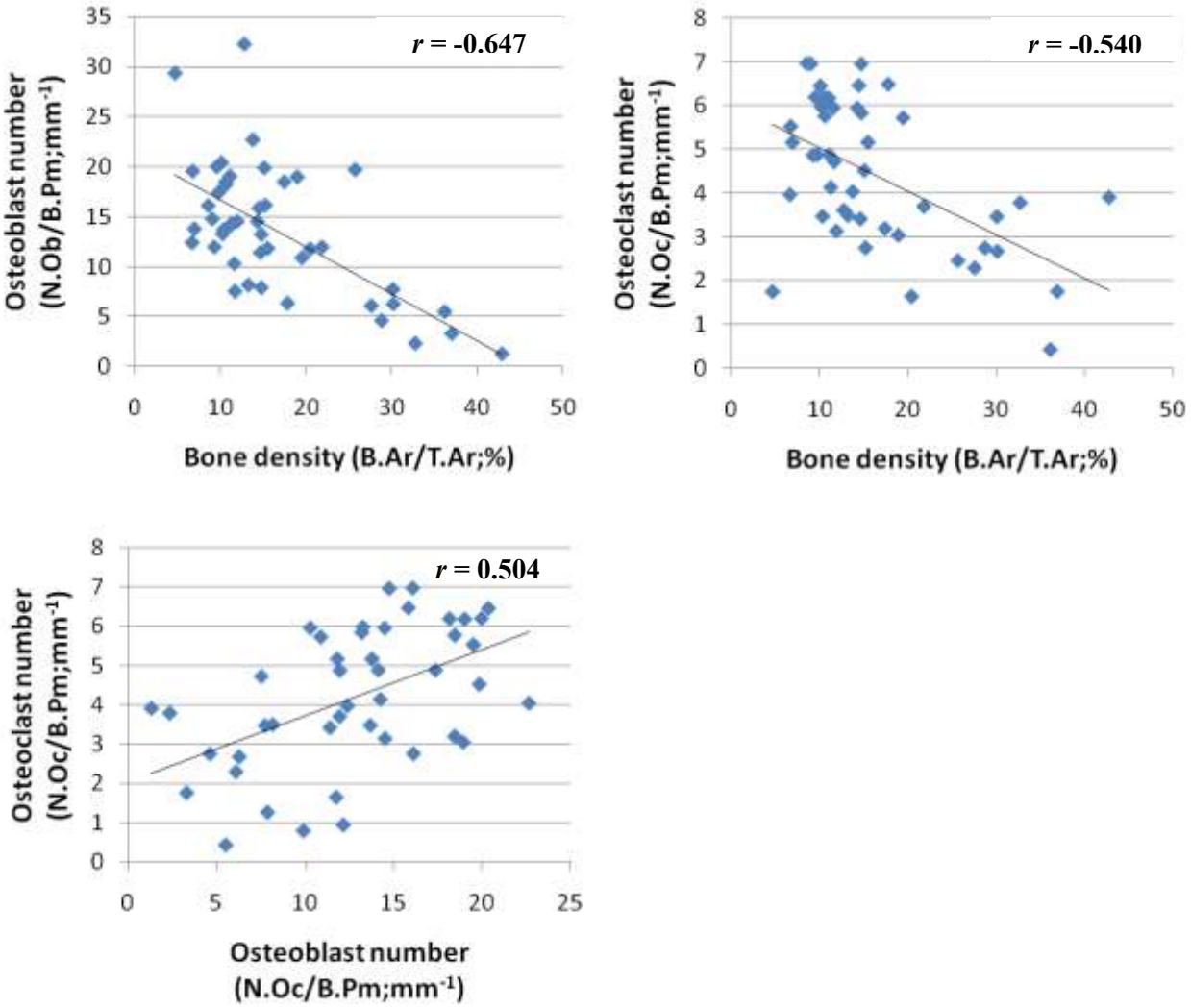

Fig.17 Scatter plots showing data sets of bone density and quantity of bone cells. The correlation between the parameters given on the X- and Y-axes are was determined by linear regression. r= reliability of linear regression.

Table 7 Structural histomophometry of primary and secondary histomorphometry

	Primary spongiosa					Secondary spongiosa				
	N	Mean	Conf.	SE	SD	N	Mean	Conf.	SE	SD
Bone density (B.Ar/T.Ar; %)										
Ctl	15	30.956	1.677	0.782	3.028	15	5.879	1.248	0.582	2.253
Het	14	29.995	3.722	1.723	6.446	14	7.449	2.202	1.019	3.814
F3	13	31.865	3.210	1.473	5.311	13	8.485	1.623	0.745	2.686
F1	14	36.223	2.850	1.319	4.936	14	13.016	3.768	1.744	6.526
KO	4	35.252	10.267	3.226	6.453	4	46.975	11.588	3.641	7.282
Trabecular thickness (Tb.Th; mm)										
Ctl	15	0.030	0.001	0.000	0.001	15	0.048	0.003	0.002	0.006
Het	14	0.030	0.002	0.001	0.004	13	0.048	0.006	0.003	0.010
F3	13	0.031	0.003	0.001	0.004	13	0.045	0.003	0.002	0.006
F1	14	0.032	0.003	0.001	0.005	14	0.044	0.002	0.001	0.004
KO	4	0.026	0.003	0.001	0.002	4	0.052	0.014	0.005	0.009
Trabecular separation (Tb.Sp; mm)										
Ctl	15	0.067	0.004	0.002	0.008	15	0.969	0.218	0.102	0.394
Het	14	0.072	0.009	0.004	0.015	14	0.757	0.146	0.068	0.254
F3	13	0.067	0.007	0.003	0.011	13	0.545	0.086	0.040	0.143
F1	14	0.058	0.005	0.002	0.008	14	0.432	0.164	0.076	0.285
KO	4	0.049	0.018	0.006	0.011	4	0.060	0.013	0.004	0.008
Trabecular number (Tb.N; mm^{-1})										
Ctl	15	10.485	0.443	0.207	0.801	15	1.199	0.192	0.089	0.346
Het	14	10.011	0.679	0.314	1.175	14	1.456	0.261	0.121	0.452
F3	13	10.332	0.627	0.288	1.037	13	1.870	0.276	0.127	0.457
F1	14	11.308	0.567	0.262	0.981	14	2.919	0.817	0.378	1.415
KO	4	13.759	3.144	0.988	1.976	4	9.055	0.140	0.044	0.088
	Growth plate thickness (mm)					Thickness of primary spongiosa (mm)				
	N	Mean	Conf.	SE	SD	N	Mean	Conf.	SE	SD
Ctl	15	0.153	0.009	0.004	0.016	15	0.327	0.017	0.008	0.031
Het	14	0.154	0.010	0.005	0.018	14	0.333	0.029	0.013	0.049
F3	13	0.152	0.018	0.008	0.029	13	0.381	0.054	0.025	0.089
F1	14	0.152	0.015	0.007	0.026	14	0.492	0.065	0.030	0.112
KO	4	0.229	0.091	0.029	0.057	4	0.419	0.169	0.053	0.107

Table 8 Bone turnover rate on inner surface of anterior and posterior cortex

MAR	Anterior cortex (µm/day)					Posterior cortex (µm/day)				
	N	Mean	Conf.	SE	SD	N	Mean	Conf.	SE	SD
Ctl	5	4,464	0,559	0,201	0,451	5	6,537	0,552	0,199	0,444
Het	9	4,327	0,548	0,238	0,713	9	7,046	1,143	0,496	1,487
F3	6	4,314	0,967	0,376	0,922	6	6,609	0,867	0,337	0,827
F1	6	4,495	0,766	0,298	0,730	6	5,445	0,813	0,316	0,774
KO	N.A.					N.A.				

MAR	Sum of both cortex (µm/day)				
	N	Mean	Conf.	SE	SD
Ctl	5	5,500	0,368	0,133	0,297
Het	9	5,686	0,747	0,324	0,972
F3	6	5,461	0,828	0,322	0,789
F1	6	4,970	0,490	0,191	0,467
KO	N.A.				

Table 9 Bone compartment fraction in ROI A and ROI B

	ROI A					ROI B				
	N	Mean	Conf.	SE	SD	N	Mean	Conf.	SE	SD
Mineralized volume (Md.Ar/T.Ar; %)										
Ctl	13	14,918	2,367	1,086	3,916	13	6,706	2,310	1,060	3,823
Het	11	17,514	3,918	1,758	5,832	11	8,642	3,661	1,643	5,450
F3	9	16,645	2,911	1,262	3,787	9	11,220	5,433	2,356	7,069
F1	13	32,904	5,211	2,392	8,623	13	20,606	6,619	3,038	10,952
KO	3	40,870	14,362	3,338	5,782	3	40,003	13,636	3,169	5,489
Osteoid volume (O.Ar/T.Ar; %)										
Ctl	13	2,795	0,983	0,451	1,627	13	6,126	2,784	1,278	4,607
Het	11	1,413	0,755	0,339	1,124	11	3,868	1,628	0,730	2,423
F3	9	2,093	0,666	0,289	0,867	9	2,533	0,976	0,423	1,269
F1	13	0,621	0,404	0,186	0,669	13	1,215	0,709	0,325	1,173
KO	3	3,978	2,559	0,595	1,030	3	4,439	5,025	1,168	2,023
Osteoid surface (OS/B.Pm; %)										
Ctl	13	10,174	2,854	1,310	4,722	13	22,034	6,947	3,189	11,496
Het	11	5,180	2,485	1,115	3,698	11	14,252	4,968	2,230	7,395
F3	9	7,258	1,568	0,680	2,039	9	11,057	4,112	1,783	5,349
F1	13	2,344	1,519	0,697	2,514	13	4,926	2,882	1,323	4,768
KO	3	10,528	5,702	1,325	2,296	3	15,260	15,770	3,665	6,348

Table10 Cellular histomorphometry in ROI A and ROI B

	ROI A					ROI B				
	N	Mean	Conf.	SE	SD	N	Mean	Conf.	SE	SD
Osteoblast bone surface density (N.Ob/B.Pm; mm^{-1})										
Ctl	13	15,812	3,402	1,561	5,629	13	24,897	6,776	3,110	11,212
Het	11	15,433	2,783	1,249	4,143	11	20,888	3,139	1,409	4,673
F3	9	13,664	2,549	1,106	3,317	9	15,625	5,560	2,411	7,233
F1	13	6,129	1,495	0,686	2,474	13	7,510	3,256	1,494	5,388
KO	3	9,134	4,611	1,072	1,856	3	10,597	7,216	1,677	2,905
Osteoblast index (N.Ob/Ob.Pm; mm^{-1})										
Ctl	13	74,302	2,544	1,168	4,210	13	80,531	3,855	1,769	6,379
Het	11	72,684	2,838	1,274	4,225	11	78,109	3,312	1,486	4,930
F3	9	76,636	4,514	1,958	5,873	9	80,715	5,131	2,225	6,675
F1	13	68,354	3,103	1,424	5,135	13	70,452	3,820	1,753	6,321
KO	3	74,086	8,178	1,901	3,292	3	74,066	8,129	1,889	3,272
Osteoclast bone surface density (N.Oc/B.Pm; mm^{-1})										
Ctl	13	4,176	0,950	0,436	1,572	13	4,575	1,052	0,483	1,740
Het	11	4,708	0,878	0,394	1,307	11	5,125	1,341	0,602	1,996
F3	9	5,244	1,193	0,517	1,552	9	6,033	1,476	0,640	1,920
F1	13	3,031	1,016	0,466	1,682	13	4,350	1,297	0,595	2,146
KO	3	0,730	0,309	0,072	0,124	3	0,897	0,421	0,098	0,169
Osteoclast index (N.Oc/Oc.Pm; mm^{-1})										
Ctl	13	39,354	2,464	1,131	4,077	13	38,116	2,028	0,931	3,355
Het	11	37,969	1,635	0,734	2,433	11	36,388	2,324	1,043	3,459
F3	9	36,232	1,795	0,778	2,335	9	35,332	3,204	1,389	4,168
F1	13	34,176	1,280	0,587	2,118	13	37,668	2,051	0,941	3,393
KO	3	28,053	10,314	2,397	4,152	3	27,141	7,493	1,742	3,016

3.5 In situ expression of proteins required for osteoclast function

In order to assess whether a correlation exists between ClC-7 protein expression and the histomorphometric parameters, immunofluorescence detection of this chloride channel in comparison to other osteoclast-expressed proteins was performed. The degree of expression of ClC-7 and the a3-subunit of the v-type H^+-ATPase varied strongly dependent on the bone region. Primary spongiosa, outer surface of posterior cortex, and some parts of the secondary ossification center rather than secondary spongiosa or inner surface of cortex were the areas in which osteoclasts exhibited high expression. ClC-7 and a3-subunit were detected in and adjacent to the ruffled membrane while β3-integrin resided at the basolateral membrane. Only expression of ClC-7, but not of the functionally related a3 subunit, was different between the groups. The intensity of ClC-7 expression was very low in F1, weak but clearly detectable in F3, and most intense in Ctl. ClC-7 expression was absent in KO.

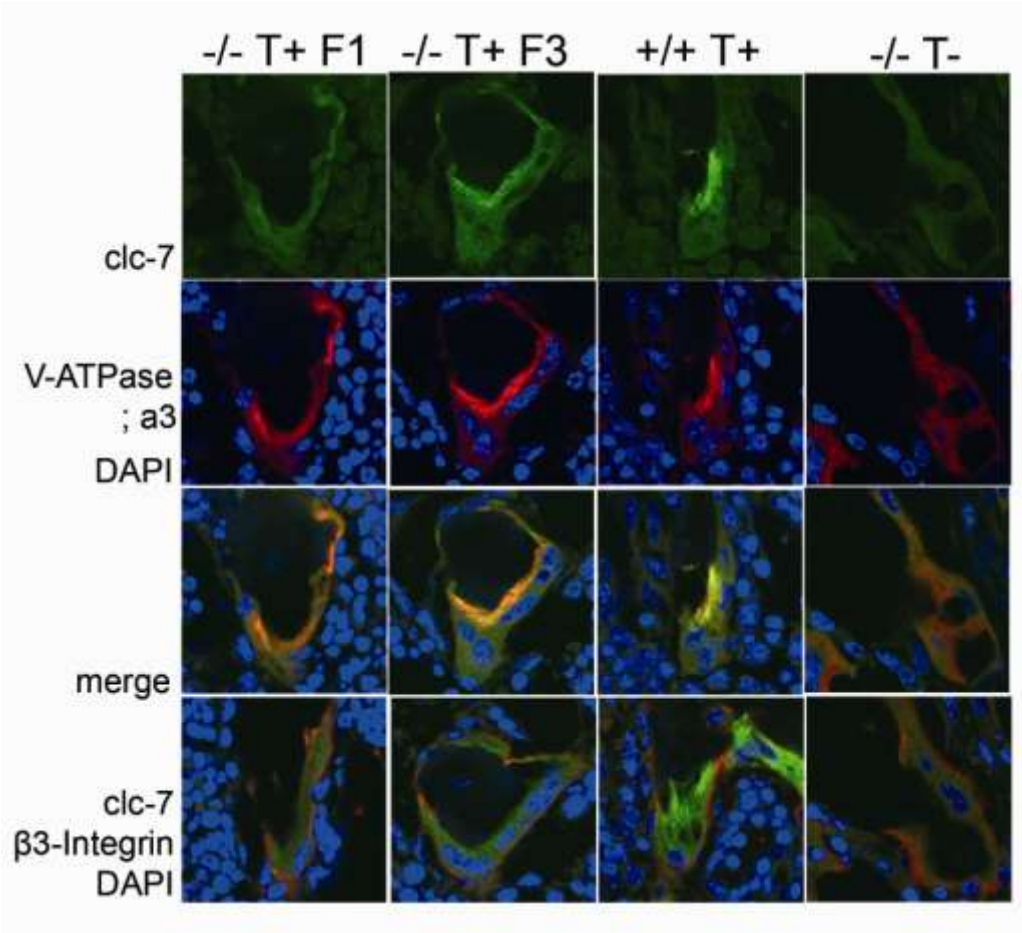

Fig.18 Confocal images of immunofluorescent detection of three proteins expressed by osteoclasts. From top: ClC-7 with Alexa Fluor® 488 (first row), a3 subunit of V0-ATPase Alexa Fluor® 555 (second row), merging of ClC-7 and a3 subunit of V0-ATPase (third row), and merging of β3-integrin with Alexa Fluor® 555 and ClC-7 with Alexa Fluor® 488 (lowest row)

3.6 Osteoclast differentiation *in vitro* study

Bone marrow and spleen cells can be induced to differentiate into mature osteoclasts in vitro by the addition of the soluble chemokines M-CSF and RANKL. Mature osteoclasts present with multiple nuclei and express TRAcP. Based on these properties, the quantification of multinucleated and TRAcP cells allows to assess osteoclast differentiation. Either percentage of multinucleated cells in F3 (8.65%, n=3) or in F1 (10.75%, n=4) were similar to Ctl (13.10%, n=3). In contrast to percentage of multinucleated cells, the percentage of TRAcP positive cells in both transgenic group (F3=32.08%, F1=25%) were significantly decreased at $p<0.05$, when compared to Ctl (51%). This result indicates that osteoclast fusion ability was not impaired, whereas TRAcP expression was attenuated in the transgenic mice.

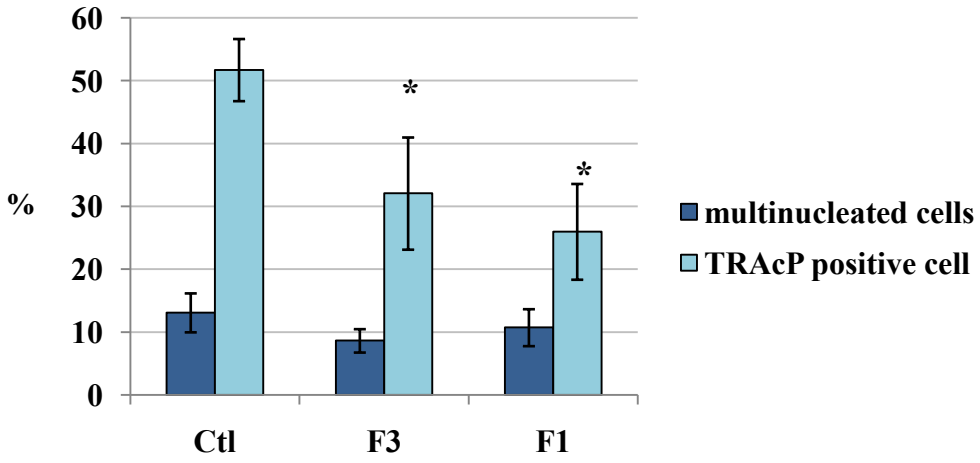

Fig.19 In vitro osteoclast differentiation, * indicates $P < 0.05$.

3.7 Gene expression at mRNA in osteoclast *in vitro* study

Osteoclasts were cultured in vitro for 2 weeks and the expression profile was determined by quantitative PCR (qPCR). The degree of osteoclast gene expression at mRNA level were first normalized by compared to the mRNA expression of endogenous gene (Gapdh), ΔC_T. Average ΔC_T of Clcn7 in Ctrl differed considerably depending on the primer pairs used. The average ΔC_T of Clcn7 using primer (6) was 15.3 cycles with a range of 10.1 to 17.9 cycles while average ΔC_T of Clcn7 using primer (8) was 4.7 with a range of 3.9 to 5.2 cycles. Afterwards, ΔC_T of Het (n=2), F1 (n=4), and F3 (n=3) were compared to Ctl (3) ($\Delta\Delta C_T$). $\Delta\Delta C_T$ of Clcn7 in both transgene groups demonstrated at very low value.

ΔΔ C_T of Clcn7 using primer pair (8) were -0.86, -9.67, and -7.93 cycles in Het, F3, and F1, respectively. And also, ΔΔ C_T of Clcn7 using primer pair (6) were -0.75, -9.02, and -9.18 cycles in Het, F3, and F1, respectively. ΔΔ C_T of Trap were only 0.28, -0.06, and -0.23 cycles in Het, F3, and F1 respectively. If these ΔΔ C_T numbers are converted into absolute values ($2^{-\Delta\Delta CT}$), the Clcn7 expression in both transgenic lines was extremely low (under 0.5% of Ctl), whereas the mRNA expression of Trap was close to normal (~120% of Ctl).

In an independent experiment, ΔΔ C_T of Clcn7 using primer pair (6) were -3.95, -10.83, and -12.37 cycles in Het, F3, and F1, respectively. In contrast, ΔΔ C_T of Ctsk were only 2.01, -2.22, and -0.53 cycles in Het, F3, and F1 respectively. In absolute values, the mRNA expression of Clcn7 in both transgenic mice was also extremely low (under 0.5% of Ctl). Ctsk expression levels were reduced in Het and F3 (~25% of Ctl), while expression was only marginally lower in F1.

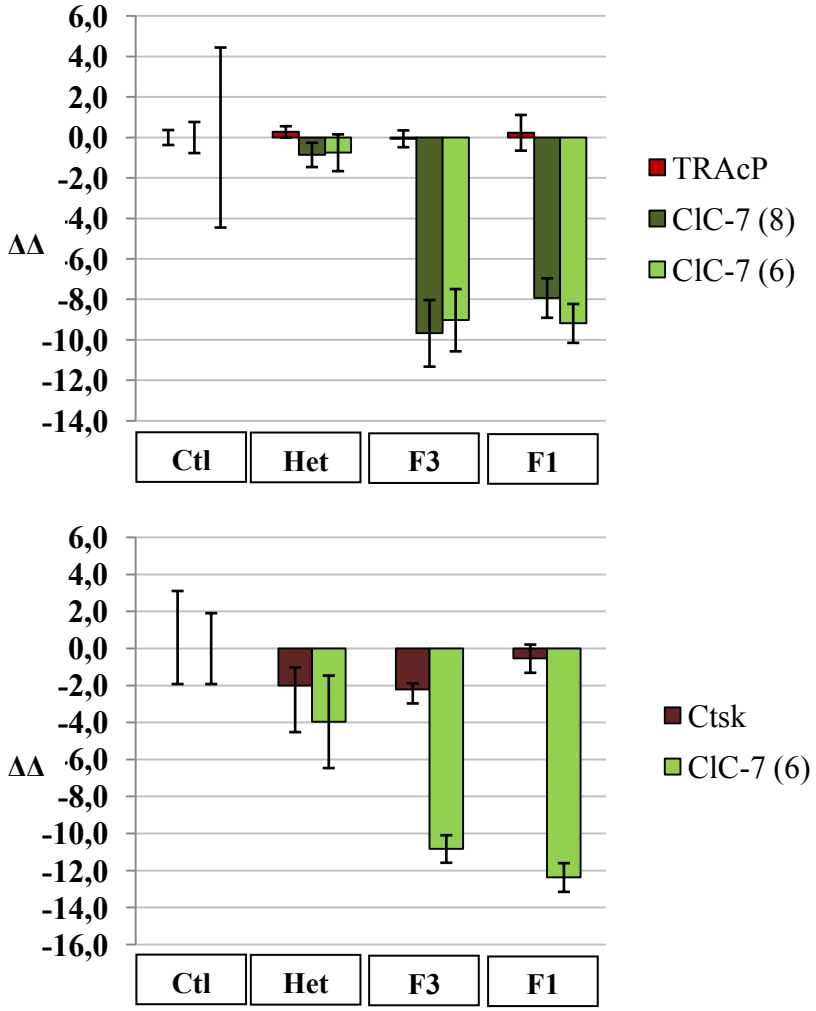

Fig.20 mRNA expression in cultured osteoclasts, bar indicates S.D.

3.8 ClC-7 expression by Western blot analysis in osteoclasts *in vitro* study

Proteins carry out the function of a gene. Levels of protein expression are not necessarily proportional to mRNA levels in a given tissue. Western blot analysis revealed that the cultured osteoclasts from both transgenic lines expressed ClC-7 at very low level when compared to the level of actin and the level of ClC-7 in Ctl. At short exposure time (5 minutes) no protein bands could be determined in F1 and F3 lanes whereas clear signals were present in Ctl lanes. Nevertheless, at the longer exposure time (20 minutes), the ClC-7 protein in the transgenic osteoclasts was detectable. The level of ClC-7 expressions in F3 was higher than in F1. Densitometric image analysis revealed that ClC-7 expression in F3 was 5.70±1.4%, while the average value in F1 was decreased to 2.51±0.89% of control signals.

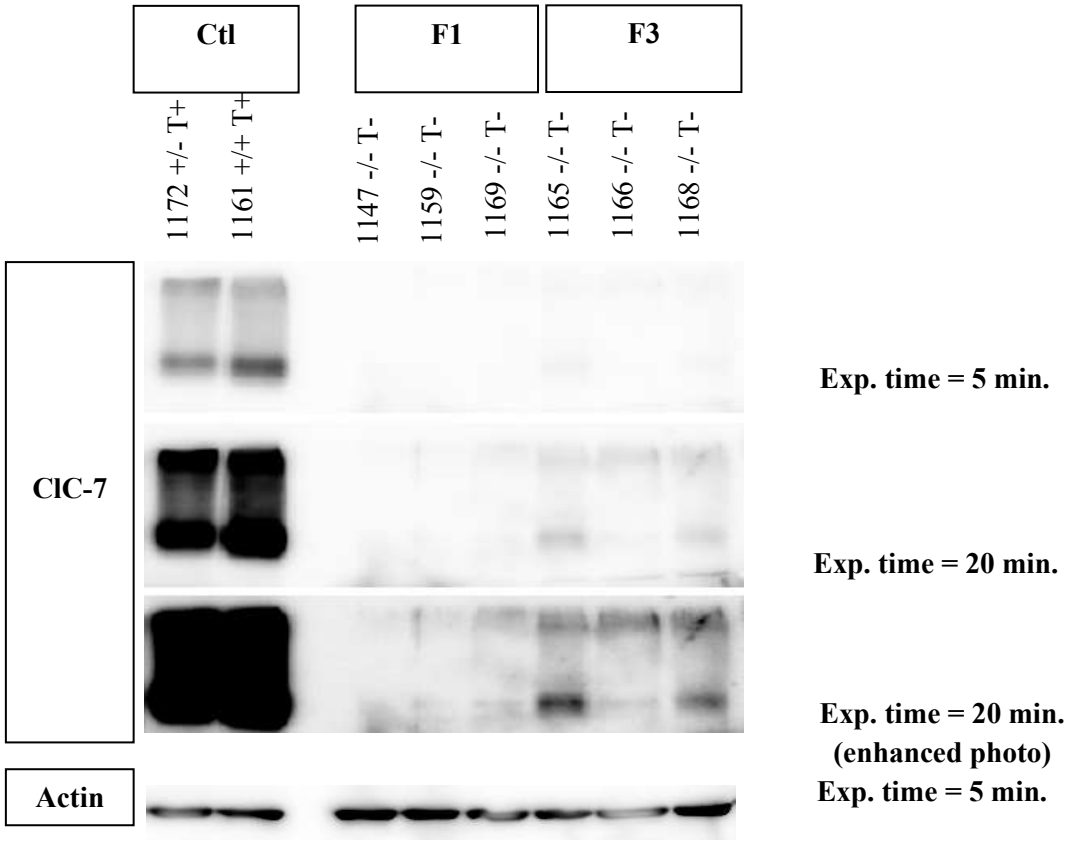

Fig.21 Inverted chemoluminescence images of Western blot analysis of ClC-7 expression

4. Discussion

4.1 Expression of ClC-7 under control of the TRAP promoter normalizes the outward appearance of *Clcn7*$^{-/-}$ mice without prolonging life expectancy.

4.1.1 Long bone growth

Complete loss of ClC-7 leads to a severe osteopetrosis phenotype resembling human infantile malignant osteopetrosis (ARO) [34]. Typically, ARO patients show a small stature due to a deficit of longitudinal growth. Growth of the long bones is dependent on growth plate function, which is not only dependent on proper proliferation of chondrocytes, but also requires resorption of hypertrophic chondrocytes. There is evidence that growth plate dysfunction in ARO is caused by insufficient mineralized cartilage resorption. On the other hand, the growth plate phenotype in ARO mouse models shows similarities to rickets, which gave rise to the term “osteopetrorickets” [94, 95]. Hypertrophic chondrocytes are resorbed by chondroclasts, which are in fact osteoclasts that resorb the mineralized cartilage. This process has been shown to be especially dependent on Mmp-9, a proteolytic enzyme active at neutral pH [96]. Given that Mmp-9 activity, in contrast to cathepsin k, does not require acid secretion by the osteoclast/chondroclast, it is surprising that the resorption of the mineralized growth plate cartilage is impaired in ARO due to mutations in proteins responsible for acid secretion. As ClC-7 is broadly expressed it could be argued that the growth plate phenotype is due to a direct effect of the loss of function on the chondrocytes. This hypothesis can be clearly rejected since mice of the *Clcn7*$^{-/-}$ T+ founder lines F1 and F3 in which TRAcP-promoter directed ClC-7 expression leads to a significant rescue of osteoclast function have normal growth of the long bones. In contrast, *Clcn7*$^{-/-}$ T+ F7 mice demonstrated an osteopetrosis phenotype identical to the phenotype of *Clcn7*$^{-/-}$ mice [34], showing that in spite of insertion of the TRAcP-ClC-7 transgenic construct into the genome there is no ClC-7 expression.

4.1.2 Tooth eruption

A second sign of osteopetrosis in mice is absent tooth eruption. This is commonly explained by a requirement of resorption of alveolar bone by osteoclasts for tooth eruption. The *Clcn7*$^{-/-}$ mice (KO) displayed a severe osteopetrosis phenotype with absence of normal eruption of incisors and molars, whereas the rescue mice (F1, and F3) displayed normal tooth eruption.

Therefore, it can be concluded that the rescue ClC-7 function of osteoclasts is able to promote normal tooth eruption. Interestingly, it has been reported that $src^{-/-}$osteopetrosis mice develop odontomas in the jaws [26, 97]. Moreover, a histomorphometric study indicated that age-related progressive increase in bone mass in $src^{-/-}$ is associated with the severity of odontomas [26]. That finding would indicate that increase in bone mass can cause the dental tumor. By contrast, the 4 week-*Clcn7*$^{-/-}$ mice (KO) displayed only a severe osteopetrosis phenotype but not odontomas. Thus, it can be suggested that the etiology of the dental tumor is not secondary to osteopetrosis.

4.1.3 Neurodegeneration

Although the rescue mice showed a normal skeletal phenotype, their weight began to decline from the 4th postnatal week onwards and had only a marginally longer life expectancy than *Clcn7*$^{-/-}$ mice. Typical abnormalities were stereotypic behavior, hind limb clasping and apathy. This can be explained by an absence of TRAcP-promoter activity in the central nervous system. Kasper et al.[93] demonstrated neurodegeneration and lysosomal storage disease in *Clcn7*$^{-/-}$ T+ mice that is comparable with the *Clcn7*$^{-/-}$ phenotype. Thus, CNS degeneration is a primary effect of ClC-7 loss and it limits life span.

Visual problems are commonly found in ARO patients and they are generally attributed to an optic canal stenosis due to the sclerosis of the skull base [98]. In spite of that, it was revealed that *Clcn7*$^{-/-}$ mice have a retinal degeneration that begins at the outer nuclear layer that contains the photoreceptors. A disturbance of the optic nerve would first result in degeneration of the ganglial cell layer on the other side of the retina that makes direct contact with the optic nerve. Again, it could be proven that this degeneration is primary because F1 and F3 rescue animals still show this phenotype although the skeletal phenotype is strongly ameliorated [93].

4.2 Static histomorphometry

4.2.1 Primary spongiosa

The primary spongiosa is formed around the longitudinal trabeculae of mineralized cartilage that are not resorbed by osteoclasts/chondroclasts at the resorption zone. The penetration of vasculature on the border of mineralized cartilage and the assistance of osteoclasts are the burden of chondrogenic bone column shaping. Suddenly after the column is successfully formed, osteoblasts will land on them and embark on apposition of newly mature bone to organize primary spongiosa. During growth, the primary spongiosa is continuously formed. With the coming of the osteoclasts to primary spongiosa, the first remodeling takes place through the simultaneous function of the osteoblasts and the osteoclasts and then leads to form mature bone, or so called secondary spongiosa. Thus, the bone quality in primary spongiosa depends on the chondrogenic bone column creation by osteoclasts and the further remodeling activity by osteoblasts and osteoclasts. Hence, the osteoclasts' dysfunction could decrease bone quality in the primary spongiosa. To observe the quality of primary spongiosa, static histomorphometric parameters were employed in a delineation of the phases of bone remodeling. All groups except *Clcn7*$^{-/-}$ shared a similar length of growth plate thickness. This finding indicates that these mice have no defect of chondrocyte differentiation and mineralization. In addition, to compare with KO growth plate, the growth plate phenotype of F1and F3 rescue mice was retrieved. There are indications that the rescue function of osteoclasts, by reinserting of *Clcn-7*, is able to resorb mineralized growth plate. Hence, it can be concluded that an acidification process by osteoclasts is required to resorb mineralized growth plate as much as MMP-9 or Cathepsin K.

In primary spongiosa, the area adjacent to the growth plate and a transitional area of premature trabeculae, high bone density in F1 rescue mice and *Clcn7*$^{-/-}$ mice indicate an atypical remodeling. As trabecular thickness is correlated to bone formation by osteoblasts, the reduced trabecular thickness in *Clcn7*$^{-/-}$ indicates a bone formation defect. Although also showing relatively high bone mass, F1 rescue mice did not have this defect. As the trabecular number and trabecular separation are the indicators of bone resorption, the decreasing trabecular separation and increasing trabecular number in F1 rescue and *Clcn7*$^{-/-}$ mice attested that the resorption function by osteoclasts in these mice is impaired. The discrepancies of trabecular separation and trabecular number between F1 and *Clcn7*$^{-/-}$ indicate that the function of F1 osteoclasts is better than that of *Clcn7*$^{-/-}$ osteoclasts. From these findings it can be concluded that osteoclast function in F1 and especially in F3 mice can be rescued by this

transgenic intervention, and that *Clcn7*$^{-/-}$ mice have impairment not only in bone resorption but also in bone formation. According to the degree of expression of ClC-7 that can be observed in immunofluorescent histology, F3, whose osteoclasts emitted higher signal of ClC-7 when compared with F1 osteoclasts, have a better primary spongiosa phenotype. Hence, it can be agreed that the level of ClC-7 can direct osteoclast function in primary spongiosa formation.

4.2.2 Secondary spongiosa

After the primary spongiosa is formed, osteoblasts and osteoclasts still collectively mold mature bone, a process that takes place in secondary spongiosa. The quality of trabeculae in secondary spongiosa is conditional on the activity of these cells. By contrast with primary spongiosa, the remodeling pattern in this stage is longer and persists evenwhen growth ceases. Secondary spongiosa acts as the secondary mineral supply for body demands. Hence, the quality of secondary spongiosa depends on systemic stimulation and can refer to a condition of systemic metabolism. On the other hand, the local function by osteoclasts and osteoblasts can also affect bone quality. If one of both cells is impaired, bone quality will be changed and as a consequence, this can alter systemic metabolism. Thus, quality of the remaining mature trabeculae can reflect on systemic status.

Compared to the primary spongiosa, increasing bone density in the secondary spongiosa in F1and *Clcn7*$^{-/-}$ mice suggests that the remodeling process is interrupted. The high bone density in F1 could be due to three reasons. First, bone deposition by osteoblasts could be accelerated. Second, bone is not properly degraded by the osteoclasts. And third, even if either osteoblasts or osteoclasts can normally form or degrade bone respectively, the transitional phase from bone formation to resorption is delayed, namely the trabeculae could not begin to be resorbed, and they could not be further formed either. In this situation, it may be on account of this that the osteoblasts have an impaired ability of coupling with osteoclast progenitor cells and allow them to land on bone for further resorption. The increasing trabecular number in of F1 indicates that the rate of bone resorption in the mice is restrained. Furthermore, the trabecular thickness and the osteoid formation in these mice were also decreased. Compared to the normal bone formation in the primary spongiosa, this indicates that the bone formation phase in F1 secondary spongiosa is torpid and at the same time, it would be turning into the early stage of the resorption phase, in which osteoclasts recently landed. The decreasing trabecular separation and increasing trabecular number in F1, F3, and

Clcn7$^{-/-}$ indicate that the resorption ability is impaired. It is possible to conclude that bone remodeling for newly secondary spongiosa of F1 is delayed by the resorption phase, while the bone remodeling in F3, Ctl, and Het can transit into formation period and well form mature spongiosa. The trabecular thickness in secondary spongiosa of *Clcn7*$^{-/-}$ was raised from lower level in primary spongiosa to the same level in secondary spongiosa. Thus, on the grounds of the gain of bone formation and complete loss of resorption ability, it can be shown that remodeling does not occur in ClC-7 knockout mice.

Implication to human osteopetrosis

Osteopetrosis is a metabolic bone disease that results in severe high bone mass on account of osteoclast dysfunction. Classification of the disease is based on severity and mode of inheritance. The most severe type of osteopetrosis is autosomal recessive (ARO), and usually detected at very early age due to its complications such as pancytopenia, upper airway obstruction, neurologic disorders etc. Most cases are caused by homozygous mutation of *TCIRG1* which encode H^+-V0-ATPase that is required for acidification in osteoclasts. On account of defect of acidification, chloride channel which is responsible for this process, has been suspected of giving rise to the disease. Strikingly, this postulation was discovered after the substantiation by Kornak et al.[34] that homozygous mutation in *CLCN7* results in loss of function of osteoclasts and leads to malignant osteopetrosis. Following the discovery of ClC-7 induced malignant osteopetrosis, there are many reports that there are also other types of osteopetrosis that result from *CLCN7* mutation [86, 87]. Interestingly, *CLCN7* mutations are found in both types, while ATP6i mutation is found only in ARO. Thus the competence of osteoclasts seems to be associated with the pattern of *CLCN7* mutation, degree of expression and the subsequent clinical characteristics.

The most common ClC-7 affected osteopetrosis is ADO II whose ~70% results from one allele mutation of *CLCN7*. The most frequent radiographic sign of ADO II is the sclerosing bone at the vertebral endplate, so called “sandwich vertebrae or rugger jersey” appearance. The band of sclerosis can be found at the metaphyses of the long bone as well as at the medial of the pelvic wings. According to radiographic findings, osteosclerosis is likely to occur at the area of high turnover rate, thus it was supposed that the ability of osteoclasts would associate with ClC-7 expression. In addition to a histomorphometry study in the ADO II, iliac crest biopsies revealed the remodeling defect due to the impaired resorption activity [85]. The

evidence that the resorption activity is impaired in ADO II is that the bone density is increased but the trabecular thickness is decreased. In an animal model, the tiny pelvic bone and vertebrae are limitation to observe the turnover rate. Seeing that primary spongiosa of growing tibia is a zone of high turnover rate in both adult human vertebral endplate and pelvic wing, the tibiae of rescue mice were chosen for the investigation of phenotype-genotype relationship. Strikingly, F1 primary spongiosa represents high bone density due to debilitated bone resorption, while F3 whose osteoclasts expressed higher ClC-7 have normal primary spongiosa phenotype. Thus, it can be concluded that owing to very low ClC-7, expression in mice leads to ADO II-like skeletal phenotype.

In case of ARO, of which 17% results from homozygous mutation of *CLCN7* gene, a severe type of osteopetrosis, the radiographic findings are general sclerosis especially at the metaphyses, the transverse expansion of metaphyses and constricted diaphyses, or sometimes called “Erlenmeyer flask” appearance. Judging by the general morphology of *Clcn7*$^{-/-}$ tibiae, the horizontal expansion at the metaphyses appears rather normal, while the diameter at diaphyses is very narrow. This finding can imply that the complete loss of osteoclast function cannot establish cortical bone formation, albeit the horizontal growth of metaphyses appears normal. Thus, it is possible to conclude that the complete loss of ClC-7 in both humans and mice leads to recessive type of osteopetrosis. According to an ARO histologic finding [99, 100], and as can be seen in the *Clcn7*$^{-/-}$ mice, they have common characteristics, i.e. the elongation of growth plate, persistence of cartilage core in primary spongiosa, and the undisrupted bone column.

4.3 Dynamic histomorphometry

Skeletal tissue is dynamic, in other words, is the tissue is continuously resorbed and reformed in cyclic pattern. This cycle, so called remodeling cycle, is needed for skeletal growth and maintains the metabolism of calcium. Delayed remodeling may retard the growth of skeletal organ and hinder the metabolism of calcium as well. Because bone remodeling has influence on bone formation and bone resorption, the delay of remodeling can be impaired by either of them. Furthermore, imbalance of the two events can lead to abnormal quality of bone. If the bone formation rate is slowet than the bone resorption rate, bone will be lost (if severe, it will turn into osteoporosis). Conversely, if the bone formation rate is higher than the resorption rate, bone will be gained, (if severe, it will turn into osteopetrosis). In the stage of new bone

formation, fresh active osteoblasts begin to form bone through secretion of nonmineralized matrix or osteoid. The matrix acts as a scaffold for mineralization. Hence, if the osteoid is successfully formed, with normal mineralization process, mature bone will be formed. By using bone labeling marker, it can directly determine the rate of bone formation. Thus, if the rate of bone formation is low by this mean, it can imply that bone formation is lower than resorption, and then there is bone loss. In contrast, if the rate is high, bone formation will be higher than resorption, and then there is bone gain.

A limit to evaluation of trabecular bone formation rate in these mice is that the bone particles were too small to measure. Nonetheless, the observation of the remodeling of cortical bone in *Clcn7*$^{-/-}$ mice, can imply that the osteoclasts and/or their resorption competency influence the formation function of the osteoblasts. Thus, cortical bone can be an area to evaluate the rate of bone formation. Mineral apposition rate (MAR) is a parameter for the evaluation of bone formation function at the mineralization period. Because of the complete disruption of cortical formation in *Clcn7*$^{-/-}$, it is impossible to assess the bone formation rate in these mice. When comparing MAR within Ctl, it is found that the rate of mineralization on the posterior endosteum is faster than on the anterior endosteum. This indicates that the mineralizing function by posterior endosteal osteoblasts is more active than the anterior one. The endosteal MAR data showed that at the posterior cortex, F1 have a slower MAR than the other group, whereas at anterior cortex the MAR is similar in all groups. This suggests that the mineralization in F1 on posterior endosteum can be sluggish as a consequence of delayed bone resorption, while at the steady stage the rate of mineralization would not be affected by this consequence.

A limit to evaluation of trabecular bone formation rate in these mice is that the bone particles were too small to measure. Nonetheless, the fact that in *Clcn7*$^{-/-}$ mice the cortical bone is severely abnormal implies that cortical bone can be an area to evaluate the effect of reduced ClC-7 levels in osteoclasts on the rate of bone formation. Because of the complete disruption of cortical formation in *Clcn7*$^{-/-}$, it is impossible to assess the bone formation rate in these mice. We found that the rate of mineralization at the posterior endosteal surface is faster than at the anterior endosteal surface. Only at the more actively bone forming posterior cortex F1 rescue mice have a lower MAR than control mice, whereas at anterior cortex the MAR is not different. This suggests that reduced ClC-7 expression in osteoclasts only becomes rate limiting at sites of high bone turnover.

4.4 *Clcn7*$^{-/-}$ T+ rescue mice from line F1 are a model for human ADOII

ARO is a severe type of osteopetrosis due to complete mutation of two alleles of *TCIRG1*or *CLCN7* genes. The mutations lead to loss of encoding of essential proteins in osteoclasts which are required for acidification process of bone resorption. Obviously the homozygous mouse models have a similar severe osteopetrosis phenotype [34, 101]. Unlike homozygous mice, heterozygous mice do not show any bone phenotype, while the mild type osteopetrosis (ADOII) is associated with the heterozygous mutation of *CLCN7*. No explanation of the genotype-phenotype between mice and humans has been found yet. Nonetheless, it was supposed that a reduced degree of acidification might be associated with the increased bone mass in ADOII [102]. A bone qualification study in ADOII suggested that BMD in mild osteopetrosis is elevated 42% above normal control [103]. That the F1 rescue mice decreasingly express ClC-7 *in vivo* and *in vitro*, it is demonstrated that the acidification ability in these mice is diminished and consequent on mildly elevated bone mass. Therefore, the F1 rescue mice show a milder form of osteopetrosis most closely resembling ADOII.

The most common radiographic sign of ADOII is sclerosis of the vertebral endplate, so called “sandwich vertebrae or rugger jersey spine”. The band of sclerosis can be found at the metaphyses of long bones as well as at the pelvic wings. The thickening of the primary spongiosa in F1 rescue mice is very likely to be the correlate of this human phenotype. However, the rescue mice only show this phenomenon in the long bones, not in the vertebrae.

It is currently under debate whether increased bone formation by osteoblasts might contribute to the increase in bone mass in ADOII. A histomorphometry study in iliac crest biopsies from ADOII patients revealed an increase in bone density and a decrease of the trabecular thickness. This indicates that the osteoclast impairment in ADOII can lead to a remodeling defect with consecutive reduced osteoblast activity [85]. In *Clcn7*$^{-/-}$ T+ animals from line F1 there are clear indications that osteoblast function is impaired: a) trabecular thickness was reduced, b) osteoblast number was low, and c) osteoid area was decreased. The dynamic evaluation in ADOII by Bollerslev et al. [85] demonstrated that the MAR as well as the resorptive indices on trabeculae of iliac bone are apparently increased. These findings suggest that the formation activity can positively regulate resorption activity. Although the osteoblast number in that study was not mentioned, the slightly elevated osteoid surface index can indicate the increase of osteoblast quantity. By contrast, F1 mice have a slower rate of mineralization due to the delayed bone resorption. This differing finding can be due to

variance of study designs in that the histomorphometry in F1 mice was focused on the growing tibia, while in the ADOII was focused on the mature iliac crest.

Another hallmark of osteopetrosis is expansion of the metaphyses and constricted diaphyses, leading to an "Erlenmeyer flask" appearance mainly of the femur. In long bones from *Clcn7*$^{-/-}$ the width of the metaphysis appears normal, while the diameter of the diaphysis is very narrow. This finding implies that in the absence of osteoclast function, cortical bone cannot be established, albeit the horizontal growth of metaphyses appears normal. In the F1 rescue animals we found no clear evidence for a long bone modeling defect. Taken together, the phenotype of F1 *Clcn7*$^{-/-}$ T+ mice can be regarded as a model for a mild variant of ADOII.

4.5 Implications for the regulation of the remodeling process

The bone remodeling process has to be kept under close control to prevent pathological deviation from optimal bone mass and geometry. Besides many systemic factors controlling remodeling, increasing evidence suggests local regulation by an interaction of stromal cells/ osteoblasts with osteoclasts within the remodeling unit. There are three main hypotheses how the osteoclast could signal to osteoblastic cells. a) There is evidence for direct interaction mediated through surface receptors. It could also involve soluble factors. The bone matrix is a reservoir for many proteins that influence osteoblast differentiation. b) As these matrix-embedded factors are liberated by osteoclast resorption, they could be part of a feedback loop by which increased resorption stimulates bone formation. However, it must be considered that a large part of these proteins will be degraded by the load of proteases secreted by the osteoclast. c) As a third possibility there is evidence for a coupling factor secreted by the osteoclast independent of resorption. As mentioned above, the data on bone formation in human ADO II is contradictory. In the F1 *Clcn7*$^{-/-}$ T+ mice we observed clearly reduced osteoid and osteoblast numbers per bone surface in the cancellous bone and a reduction of the mineral apposition rate in the cortical bone, all indicative of reduced bone formation. It must be taken into account that also the osteoclast number per bone surface is reduced in F1 rescue mice. However, although the maximum reduction of osteoclasts is 25% in ROI A the osteoblasts numbers are decreased by 60%. This indicates that the reduced resorptive activity plays a decisive role in the regulation of osteoblast numbers in the trabecular bone. This interpretation is further supported by the fact that in F3 rescue mice osteoblast numbers are also mildly reduced in spite of the fact that osteoclast numbers are even slightly elevated.

What is the factor that controls the number of osteoblasts in the proximal region? The retention of osteoblasts depends on the rate of differentiation and the fade of mature osteoblasts. Runx2 is the pivotal transcription factor that decides the fate of osteoblast differentiation. The activation of Runx2 allows preosteoblasts differentiate to mature osteoblasts and inhibits mature osteoblasts from transforming into osteocytes [7, 104]. Runx2 can be activated by TGF-β/Smad pathway and Wnt signaling pathway. Clearly, TGF-β superfamily and it members as known as bone morphogenetic proteins (BMPs) are major osteogenic proteins. In developmental stage, TGF-β is mostly secreted from cells. It has been postulated that the factors would be entombed in the mature bone during formation period. To answer the hypothesis, it was shown that the source of TGF-β is in the degraded bone resulting from resorption process and required for bone remodeling [105, 106]. Hence, the defect in bone resorption can decrease the osteoblast differentiation via TGF-β and suppress the bone formation rate. On the other hand, in canonical Wnt pathway, β-catenin can mediate the osteoblast differentiation through the Runx2, and also regulates the survival of mature osteoblasts through β-catenin/LEF1 signal. Sclerostin, an antagonist of Wnt can prevent the extracellular binding of Wnt to the Fz-LRP5/6 complex that leads to the degradation of β-catenin. This molecule is highly expressed in osteocytes, canaliculi, their surrounding bone, and hypertrophic chondrocytes [107-109]. At the osteon presenting stage, the sclerostin causes the unstable β-catenin, therefore the mature osteoblasts will be induced to apoptosis. Thus, as the consequence of inadequate bone resorption in F1, the sclerostin from the remaining osteocytes and its surrounding bone, as well as the low TGF-β signal, could inhibit the osteoblast differentiation and trigger apoptosis of the osteoblasts.

To summarize the remodeling event in F1, firstly, the remodeling of newly formed bone in primary spongiosa would be interfered with by the impaired function of osteoclasts to appropriately resorb the chondrogenic bone columns. Then, the osteoblasts were induced to apoptosis, and the coupling signals to initiate osteoclastogenesis from osteoblast would be dropped. The limited number and properties of the osteoclasts suspends the bone resorption. Even if the bidirectional signal from the osteoclasts could introduce the preosteoblasts to transit to the formation phase, the sclerostin and the low TGF-β at this stage would rather prevent the proper differentiation of the osteoblasts. Then the next cycle of bone remodeling would be affected by inadequate the functioning of the osteoclasts. It is possible to conclude that the delayed bone remodeling in F1 results from impaired osteoclast function and delayed coupling mechanism. Furthermore, the limited bone resorption can indirectly delay the differentiation of osteoclasts and osteoblasts.

Osteoclast numbers and osteoblast numbers in *Clcn7*$^{-/-}$ were obviously low in both regions. Because of the complete loss of bone resorptive function, the bone remodeling could not be established. Two reasons can be given to explain why the osteoblast and osteoclast differentiation was severely blocked. First, an increase in bone density causes a blockade of vascular invasion that obstructs accesses of osteoclasts migration, and a reduction of marrow space that reduces stromal cells proliferation. Second, the nonresorbing bone blocks the coupling process of the bone cells. Notably, the osteoblast number of *Clcn7*$^{-/-}$ was higher than F1 though the bone remodeling was more severe. The hyperplastic chondrocytes in *Clcn7*$^{-/-}$ were higher than usual. This can imply that the level of β-catenin might be reduced by high sclerostin in hyperplastic chondrocytes. The diminished level of β-catenin at the chondroosseous junction would prevent osteocyte transformation and reduce bone formation. If the number of osteocytes would be reduced as a consequence, the low signal from osteocytes could reduce the osteoblast number.

As can be seen in Table.11, the bone formation marker level in all available studies of ADOII is elevated, while bone resorption marker level is also elevated in 3 of 5 studies. Notably, only one available study which observed in histomorphometry in ADOII shows an increase of number and size of osteoclasts[110]. Since bone mass corresponds to bone surface, the rise of bone resorption index in ADOII could be accounted for the plenteous bone surface, albeit the function of osteoclast is normal or abnormal. It may indicate that the excess of bone resorption marker level is due to the negative feedback from bone formation rather than to the ability of the osteoclasts. Moreover, the explanation can be supported by the in vitro study that showed that ADOII isolated osteoclasts have reduction ability in bone resorption [111]. Thus, it can be concluded that the bone turnover rate in ADOII is high as a result of compensation of the osteoclastogenesis induction. It is in contrast to the turnover prolonged rate in F1. The contradiction of remodeling pattern between ADOII and F1 can be explained by the fact that the elevated TGF-β level in ADOII induces the differentiation of osteoblasts. In F1 study, although bone formation marker was not involved and the osteoblast number was low, it could not be shown that F1 has low bone formation. F1 bone formation was designed to be investigated in development stage, while most of ADOII bone remodeling studies focused on aged patients [87, 110-114]. Bone formation in the development stage are resulted from two events namely by chondrogenic bone formation for growth and osteogenic (osteoblasts) bone formation for remodeling of mature bone. Because at this stage, bone is formed dominantly by chondrocytes, thus the reduction of osteoblast activation might be

suppressed, though a high bone formation rate is present. This is supported by the thickness of primary spongiosa which was particularly high in F1.

Table 11 Summary of bone remodeling studies in osteopetrosis

Osteopetrosis type ; study design (authors)	Demographic data	Biochemistry		Histological findings			Mutated gene
		Resorption index	Formation index	General structure	Osteoclast activity	Osteoblast activity	
ARO ; 4 cases (Taranta et al.)[115]	4 cases Birth to 18 yr.		↑↑ ALP	↑ bone density, irregular shape of Tb., myelofibrosis, ↓ stromal cells	↑ size, ↑ nuclei ↓↓↓ pit formation (*in vitro*)		*ATP6i*
; (Helfrich et al.)[116]	6 cases 1.5-6 mth	↑ AP	↑↑ ALP	no amorphous formation	↑↑ N.Oc, Normal osteoclast structure (US)	↓↓ N.Ob	NI
; case report (Shapiro et al.)[99]	a 3-mth female		↑↑ ALP	↑↑ cartilage core, ↑ bone density	↑↑ N.Oc, ↑ size, ↑ nuclei	↓↓ N.Ob	NI
; (Reeves et al.)[117]	5 cases 8-22 mth	↓ Hyp	↑ ALP	↑ osteoid, myelofibrosis	↑↑ N.Oc, ↑ size	→N.Ob	NI
; (Del Fattore et al.)[87]	17 cases 3-24 yr.		↑↑ ALP	Pit index = ~8% of control (*in vitro*)	Variable in number	↑ N.Ob if ↑N.Oc	*ATP6i* (5 in 9 cases)

Legends: ↑; increase, ↓; decrease, →; not changed, AP; acid phosphatase, ALP; alkaline phosphatase, β-CL; β-Crosslap, α-CL; α-Crosslap, CTX; carboxyterminal telopeptide of type I collagen, D-Pyr; free deoxypyridinum crosslinks, NI; not investigated, OCN; osteocalcin, SLAP; bone-specific leptin-precipitated alkaline phosphatase, Tb; trabeculae, TRAcP ; Tartrate-resistant acid phosphatase, US; ultrastructure, Hyp; urine hydroxyproline

Osteopetrosis type ; study design (authors)	Demographic data	Biochemistry		Histological finding			Mutated gene
		Resorption index	Formation index	General structure	Osteoclast activity	Osteoblast activity	
ADO I ; (Bollerslev et al.)[110, 112]	5 female, 3 male 23-61 yr.	↓ CTX → D-Pyr	↓ OCN ↓ SLAP		↓ N.Oc, ↓ size, ↓ nuclei, ↓ TRAP staining		NI
ADO II ; case report (Senel et al.)[114]	1 case 23 yr., male	↑ AP	↑ ALP				NI
; in vitro (Henriksen et al.)[111]	9 cases 28-60 yr.	↓↓ CTX	NI				*CLCN-7*
; case report (Letizia et al.)[118]	1 case 16 yr. male	↑↑ CTX	↑ ALP ↑ OCN				*CLCN-7*
; case report (Semba et al.)[113]	1 case 61 yr. male			Osteomyelitis, irregular apposition pattern, ↑ amorphous content	Prolong demineralization, ↑↑ lysosomal vesicle (US)		NI
; (Bollerslev et al.)[110, 112]	3 females, 6 males 20-49 yr.	→ CTX, D-Pyr, β-CL, α-CL ↑↑ TRAcP (n=7)	→ OCN → SLAP ↓ ALP (n=6) ↑ OCN (n=10)		↑↑ N.Oc, ↑ size, ↑ nuclei		NI
; (Del Fattore et al.)[87]	20 patients 3-63 yr.			Pit index = ~30% of control (*in vitro*)			*CLCN-7* (~70% of cases)

4.6 ClC-7 expression levels influence bone mass

Loss of ClC-7 causes ARO in humans and mice due to a complete loss of bone resorption indicating that ClC-7 is crucial for osteoclast function [34]. In contrast to the recessive loss of function mutations in ARO dominant mutations, the amount of functional ClC-7 dimers in ADOII is reduced to maximal 25%. Accordingly, several studies [87, 102, 111] showed that osteoclasts from *CLCN7* ADOII patients only have a reduced resorptive capacity. Although there is currently no evidence for increased bone mass in heterozygous carriers of ARO mutations in which ClC-7 function is reduced to 50%, $Clcn7^{+/-}$ mice show changes that mimic a minimal form of osteopetrosis. Furthermore, two independent studies demonstrated that sequence polymorphisms in *CLCN7* are associated with bone mass, although they can only have very mild effects on ClC-7 function [119, 120].

Although in humans already a reduction of ClC-7 function to approx. 25% leads to a resorption deficit that causes ADOII, osteoclasts from $Clcn7^{+/-}$T+ rescue mice from lines F1 and F3 both show only mild osteopetrosis in spite of expression levels far below 10%. Interestingly, in line F3, osteoclasts derived from bone marrow cells and spleen cells expressed higher ClC-7 than in lines F1 (approx. 5.7% in F3, 2.5% in F1). Since the degree of bone mass of line F1 is higher than F3, which has almost a normal phenotype, the gap of ClC-7 expression level indicates regressive function of resorption. The very low expression of ClC-7 in lines F1 and F3 would be explained as follow: a) *in vitro* study of osteoclastogenesis revealed decreasing property of mature osteoclasts in lines F1 and F3. Hence, the ClC-7 expression would be proportionally reduced. b) Although TRAcP is very strongly specific to osteoclasts, the transgenic manipulation can allow Clcn7 cDNA with TRAcP promoter in a complex milieu. Therefore, the expression of ClC-7 would rely on the incidence of the activation of the promoter. Whatever it can be, the very low *in situ* signal of ClC-7 in line F1 osteoclasts can be comparable. As the associated phenotype, it is indicated that line F1 mice have impaired bone resorption due to very low ClC-7 expression. From these findings, it can be concluded that: a) human and mouse share the same pattern of development of osteopetrosis (Fig.22). b) The critical threshold level of ClC-7 expression is dependent on species. On account of recessive inheritance in ADOII, the osteoclast function required 25% of ClC-7 expression. If 10% expression of ClC-7 in mice is a threshold for development of osteopetrosis, it would be an explanation that the *Clcn7* heterozygous mutation in mice does not result in the phenotype.

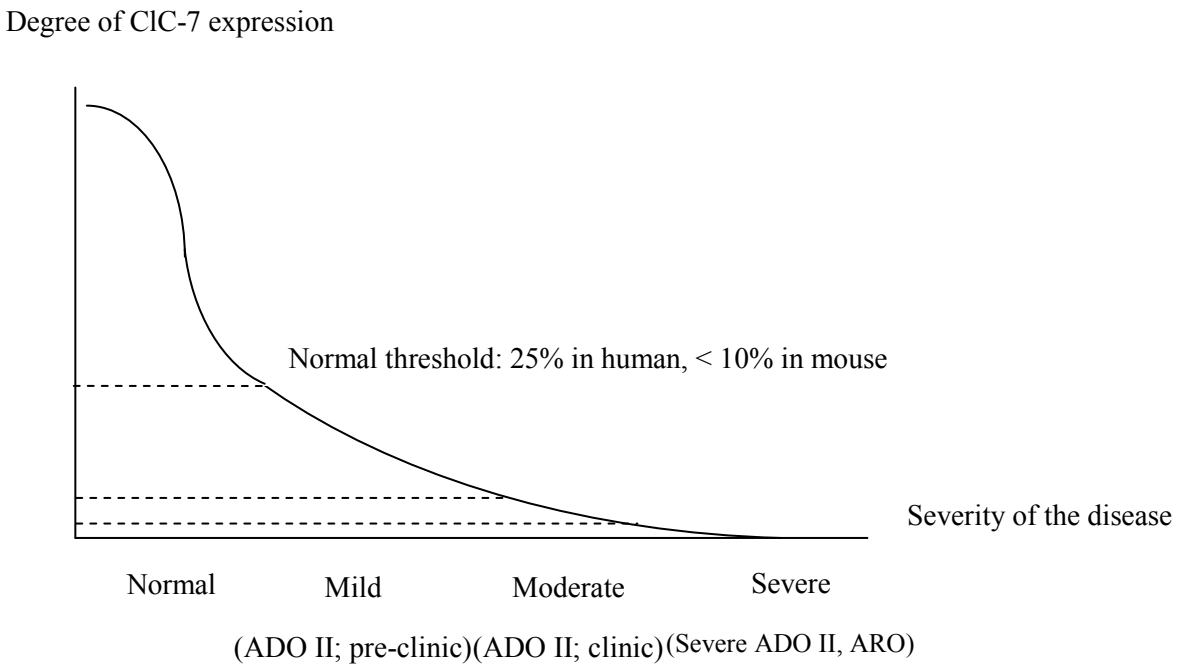

Fig.22 A proposed model of ClC-7 expression and the relevant phenotypes

4.7 Anabolic effect from nonresorbing osteoclasts

Bone formation markers in all ARO studies are elevated. This could be due to a) an increase in osteoblast function or b) just because the surface of the osteopetrotic bone is increased. Furthermore, data from one study demonstrated that all ARO cases whose osteoclast number (Oc.S/BS) is elevated have a higher osteoblast number (Ob.S/BS) [87]. Therefore, it was suggested that the elevated nonresorbing osteoclasts in osteopetrosis could induce the differentiation of osteoblasts [65]. Because of this, it was to be expected that the increased bone density in F1 and *Clcn7*$^{-/-}$ would entail increased osteoclast numbers. In contrast to this, the osteoclast number was reduced in F1 rescue animals. However, a plot of osteoclast number against osteoblast number of all samples (Ctl, Het, F1, F3, and Clcn7-/-) revealed a slight correlation. It therefore seems that the correlation of osteoblast and osteoclast numbers is reproduced in the mouse model, but that, in contrast to human ARO, the osteoclast numbers in the trabecular bone of the tibia are decreased. The different result between ARO and *Clcn7*$^{-/-}$ (KO) mice would be explained by the fact that most cases of ARO whose osteoclasts number is elevated are of very young age, while the KO mice were investigated at a later stage of development after the growth spurt. Furthermore, another study describing osteopetrosis cases of a wide age range (3-27 years old) revealed highly variable osteoclast numbers [87]. Moreover,

many histomorphometric analyses do not describe the cell numbers in relation to the bone surface. As bone surface is necessarily increased in osteopetrosis, total numbers of osteoblasts and osteoclasts are also elevated. It must also be considered that the human bone specimens are derived from the iliac crest while the mouse bone analyzed in this study was the tibia. Therefore, it is currently difficult to reconcile the partial differences between our mouse model and the findings in human patients.

4.8 Conclusion and perspective aspect

ClC-7 is essential for osteoclasts to maintain electroneutrality during bone resorption. Complete loss of ClC-7 in *Clcn7*-/- mice and *CLCN7* mutation in humans lead to severe osteopetrosis phenotype. Heterozygous mutation can cause a mild osteopetrosis in human (ADO II) but not in mice. The pattern of phenotype expression would be distinguished between the species. It has been expected that the ClC-7 level would affect the phenotype. The present study shows that the level of ClC-7 expression correlates with bone resorbing competency of osteoclasts. Heterozygous and F3 mice have a higher ClC-7 level than F1 mice which have more severe bone phenotype. The margin of ClC-7 expression to develop osteopetrosis would be at 2-7% in mice and 25% in human. From this finding, to maintain ClC-7 above the margin in individuals at high risk of mild osteopetrosis would be a preventive strategy of the disease.

ARO is lethal, unless the disease is detected early. Mutation in *CLCN7* is a cause of the disease [34]. The treatment of choice in severe ARO is only allogeneic haematopoietic stem cell transplantation (HSCT) so far. Prognosis of this disease is still very poor, although the patients have been tried to treat by HSCT. The survival rate after HSCT is low (from 40% to 80) [89, 121-123]. The present study shows that the recovery of ClC-7 under the control of TRAcP promoter in *Clcn7-/-* mice can rescue bone phenotype. Hence it would be implied that further gene therapy in ClC-7 deficient osteopetrosis by rescued osteoclasts would cure the bone disease. By this means, the neurodegeneration was not retrieved. Thus the treatment of neurodegeneration would be achieved by another gene therapeutic strategy rather than osteoclasts specific gene treatment.

Osteoporosis is a degenerative metabolic bone disease due to hyperactivity of osteoclasts or hypoactivity of osteoblasts. The progressive bone loss is strongly associated with the menopause. Women in this period have lower production of the reproductive hormones such as estrogen and

progesterone. The menopause women who lack the hormones have been prescribed with supplement hormone to prevent unfavourable complications associated with osteoporosis. The long-term hormone replacement therapies have been concerned for risk of breast cancer and cardiovascular diseases [124-128]. Bisphosphonates are also favored to reduce risk of fracture in postmenopausal osteoporosis. The bisphosphonates can irritate gastrointestinal tract and increase the risk of jaw osteonecrosis. Once nonresorbing osteoclasts can be regulated by modification of medication or gene therapy, the crosstalk between osteoclasts and osteoblasts would enable an anabolic effect in bone metabolism. Because ClC-7 is very expressed in osteoclasts, repression of ClC-7 function would decrease bone turnover and be beneficial for reducing complications of osteoporosis with minimal adverse effects.

5. References

1. Clapham DE. Calcium signaling. Cell 1995;80:259-68.
2. Manolagas SC. Birth and death of bone cells: basic regulatory mechanisms and implications for the pathogenesis and treatment of osteoporosis. Endocr Rev 2000;21:115-37.
3. Long MW, Robinson JA, Ashcraft EA, Mann KG. Regulation of human bone marrow-derived osteoprogenitor cells by osteogenic growth factors. J Clin Invest 1995;95:881-7.
4. Reilly TM, Seldes R, Luchetti W, Brighton CT. Similarities in the phenotypic expression of pericytes and bone cells. Clin Orthop Relat Res 1998;95-103.
5. Rickard DJ, Kassem M, Hefferan TE, Sarkar G, Spelsberg TC, Riggs BL. Isolation and characterization of osteoblast precursor cells from human bone marrow. J Bone Miner Res 1996;11:312-24.
6. Otto F, Lubbert M, Stock M. Upstream and downstream targets of RUNX proteins. J Cell Biochem 2003;89:9-18.
7. Nakashima K, de Crombrugghe B. Transcriptional mechanisms in osteoblast differentiation and bone formation. Trends Genet 2003;19:458-66.
8. Day TF, Guo X, Garrett-Beal L, Yang Y. Wnt/beta-catenin signaling in mesenchymal progenitors controls osteoblast and chondrocyte differentiation during vertebrate skeletogenesis. Dev Cell 2005;8:739-50.
9. Hill TP, Spater D, Taketo MM, Birchmeier W, Hartmann C. Canonical Wnt/beta-catenin signaling prevents osteoblasts from differentiating into chondrocytes. Dev Cell 2005;8:727-38.
10. Yang X, Matsuda K, Bialek P, et al. ATF4 is a substrate of RSK2 and an essential regulator of osteoblast biology; implication for Coffin-Lowry Syndrome. Cell 2004;117:387-98.
11. Franz-Odendaal TA, Hall BK, Witten PE. Buried alive: how osteoblasts become osteocytes. Dev Dyn 2006;235:176-90.
12. Borton AJ, Frederick JP, Datto MB, Wang XF, Weinstein RS. The loss of Smad3 results in a lower rate of bone formation and osteopenia through dysregulation of osteoblast differentiation and apoptosis. J Bone Miner Res 2001;16:1754-64.
13. Jilka RL, Weinstein RS, Bellido T, Parfitt AM, Manolagas SC. Osteoblast programmed cell death (apoptosis): modulation by growth factors and cytokines. J Bone Miner Res 1998;13:793-802.

14. McCarthy TL, Chang WZ, Liu Y, Centrella M. Runx2 integrates estrogen activity in osteoblasts. J Biol Chem 2003;278:43121-9.
15. Tobimatsu T, Kaji H, Sowa H, et al. Parathyroid hormone increases beta-catenin levels through Smad3 in mouse osteoblastic cells. Endocrinology 2006;147:2583-90.
16. Anderson HC. Vesicles associated with calcification in the matrix of epiphyseal cartilage. J Cell Biol 1969;41:59-72.
17. Boskey AL, Moore DJ, Amling M, Canalis E, Delany AM. Infrared analysis of the mineral and matrix in bones of osteonectin-null mice and their wildtype controls. J Bone Miner Res 2003;18:1005-11.
18. Hunter GK, Goldberg HA. Nucleation of hydroxyapatite by bone sialoprotein. Proc Natl Acad Sci U S A 1993;90:8562-5.
19. Fleisch H, Straumann F, Schenk R, Bisaz S, Allgower M. Effect of condensed phosphates on calcification of chick embryo femurs in tissue culture. Am J Physiol 1966;211:821-5.
20. Anderson HC, Reynolds JJ. Pyrophosphate stimulation of calcium uptake into cultured embryonic bones. Fine structure of matrix vesicles and their role in calcification. Dev Biol 1973;34:211-27.
21. Matsumoto M, Kogawa M, Wada S, et al. Essential role of p38 mitogen-activated protein kinase in cathepsin K gene expression during osteoclastogenesis through association of NFATc1 and PU.1. J Biol Chem 2004;279:45969-79.
22. Ikeda F, Nishimura R, Matsubara T, et al. Critical roles of c-Jun signaling in regulation of NFAT family and RANKL-regulated osteoclast differentiation. J Clin Invest 2004;114:475-84.
23. Kim MS, Day CJ, Selinger CI, Magno CL, Stephens SR, Morrison NA. MCP-1-induced human osteoclast-like cells are tartrate-resistant acid phosphatase, NFATc1, and calcitonin receptor-positive but require receptor activator of NFkappaB ligand for bone resorption. J Biol Chem 2006;281:1274-85.
24. Hirotani H, Tuohy NA, Woo JT, Stern PH, Clipstone NA. The calcineurin/nuclear factor of activated T cells signaling pathway regulates osteoclastogenesis in RAW264.7 cells. J Biol Chem 2004;279:13984-92.
25. Kim K, Kim JH, Lee J, et al. Nuclear factor of activated T cells c1 induces osteoclast-associated receptor gene expression during tumor necrosis factor-related activation-induced cytokine-mediated osteoclastogenesis. J Biol Chem 2005;280:35209-16.

26. Amling M, Neff L, Priemel M, Schilling AF, Rueger JM, Baron R. Progressive increase in bone mass and development of odontomas in aging osteopetrotic c-src-deficient mice. Bone 2000;27:603-10.
27. McHugh KP, Hodivala-Dilke K, Zheng MH, et al. Mice lacking beta3 integrins are osteosclerotic because of dysfunctional osteoclasts. J Clin Invest 2000;105:433-40.
28. Gay CV, Mueller WJ. Carbonic anhydrase and osteoclasts: localization by labeled inhibitor autoradiography. Science 1974;183:432-4.
29. Vaananen HK, Parvinen EK. High active isoenzyme of carbonic anhydrase in rat calvaria osteoclasts. Immunohistochemical study. Histochemistry 1983;78:481-5.
30. Blair HC, Teitelbaum SL, Ghiselli R, Gluck S. Osteoclastic bone resorption by a polarized vacuolar proton pump. Science 1989;245:855-7.
31. Sundquist K, Lakkakorpi P, Wallmark B, Vaananen K. Inhibition of osteoclast proton transport by bafilomycin A1 abolishes bone resorption. Biochem Biophys Res Commun 1990;168:309-13.
32. Vaananen HK, Karhukorpi EK, Sundquist K, et al. Evidence for the presence of a proton pump of the vacuolar H(+)-ATPase type in the ruffled borders of osteoclasts. J Cell Biol 1990;111:1305-11.
33. Shibata T, Sakai H, Nakamura F, Shioi A, Kuno M. Differential effect of high extracellular Ca2+ on K+ and Cl- conductances in murine osteoclasts. J Membr Biol 1997;158:59-67.
34. Kornak U, Kasper D, Bosl MR, et al. Loss of the ClC-7 chloride channel leads to osteopetrosis in mice and man. Cell 2001;104:205-15.
35. Teti A, Blair HC, Teitelbaum SL, et al. Cytoplasmic pH regulation and chloride/bicarbonate exchange in avian osteoclasts. J Clin Invest 1989;83:227-33.
36. Saftig P, Hunziker E, Wehmeyer O, et al. Impaired osteoclastic bone resorption leads to osteopetrosis in cathepsin-K-deficient mice. Proc Natl Acad Sci U S A 1998;95:13453-8.
37. Gowen M, Lazner F, Dodds R, et al. Cathepsin K knockout mice develop osteopetrosis due to a deficit in matrix degradation but not demineralization. J Bone Miner Res 1999;14:1654-63.
38. Chen W, Yang S, Abe Y, et al. Novel pycnodysostosis mouse model uncovers cathepsin K function as a potential regulator of osteoclast apoptosis and senescence. Hum Mol Genet 2007;16:410-23.

39. Johnson MR, Polymeropoulos MH, Vos HL, Ortiz de Luna RI, Francomano CA. A nonsense mutation in the cathepsin K gene observed in a family with pycnodysostosis. Genome Res 1996;6:1050-5.
40. Gelb BD, Shi GP, Chapman HA, Desnick RJ. Pycnodysostosis, a lysosomal disease caused by cathepsin K deficiency. Science 1996;273:1236-8.
41. Uusitalo H, Hiltunen A, Soderstrom M, Aro HT, Vuorio E. Expression of cathepsins B, H, K, L, and S and matrix metalloproteinases 9 and 13 during chondrocyte hypertrophy and endochondral ossification in mouse fracture callus. Calcif Tissue Int 2000;67:382-90.
42. Ljusberg J, Ek-Rylander B, Andersson G. Tartrate-resistant purple acid phosphatase is synthesized as a latent proenzyme and activated by cysteine proteinases. Biochem J 1999;343 Pt 1:63-9.
43. Minkin C. Bone acid phosphatase: tartrate-resistant acid phosphatase as a marker of osteoclast function. Calcif Tissue Int 1982;34:285-90.
44. van de Wijngaert FP, Burger EH. Demonstration of tartrate-resistant acid phosphatase in un-decalcified, glycolmethacrylate-embedded mouse bone: a possible marker for (pre)osteoclast identification. J Histochem Cytochem 1986;34:1317-23.
45. Hammarstrom LE, Hanker JS, Toverud SU. Cellular differences in acid phosphatase isoenzymes in bone and teeth. Clin Orthop Relat Res 1971;78:151-67.
46. Wergedal JE. Characterization of bone acid phosphatase activity. Proc Soc Exp Biol Med 1970;134:244-7.
47. Yam LT. Clinical significance of the human acid phosphatases: a review. Am J Med 1974;56:604-16.
48. Schindelmeiser J, Schewe P, Zonka T, Munstermann D. Histochemical and immunological demonstration of purple acid phosphatase in human and bovine alveolar macrophages. Histochemistry 1989;92:81-5.
49. Hayman AR, Bune AJ, Cox TM. Widespread expression of tartrate-resistant acid phosphatase (Acp 5) in the mouse embryo. J Anat 2000;196 (Pt 3):433-41.
50. Hayman AR, Bune AJ, Bradley JR, Rashbass J, Cox TM. Osteoclastic tartrate-resistant acid phosphatase (Acp 5): its localization to dendritic cells and diverse murine tissues. J Histochem Cytochem 2000;48:219-28.
51. Hayman AR, Macary P, Lehner PJ, Cox TM. Tartrate-resistant acid phosphatase (Acp 5): identification in diverse human tissues and dendritic cells. J Histochem Cytochem 2001;49:675-84.

52. Clark SA, Ambrose WW, Anderson TR, Terrell RS, Toverud SU. Ultrastructural localization of tartrate-resistant, purple acid phosphatase in rat osteoclasts by histochemistry and immunocytochemistry. J Bone Miner Res 1989;4:399-405.
53. Lucht U. Acid phosphatase of osteoclasts demonstrated by electron microscopic histochemistry. Histochemie 1971;28:103-17.
54. Fukushima O, Bekker PJ, Gay CV. Ultrastructural localization of tartrate-resistant acid phosphatase (purple acid phosphatase) activity in chicken cartilage and bone. Am J Anat 1991;191:228-36.
55. Reinholt FP, Widholm SM, Ek-Rylander B, Andersson G. Ultrastructural localization of a tartrate-resistant acid ATPase in bone. J Bone Miner Res 1990;5:1055-61.
56. Halleen JM, Raisanen S, Salo JJ, et al. Intracellular fragmentation of bone resorption products by reactive oxygen species generated by osteoclastic tartrate-resistant acid phosphatase. J Biol Chem 1999;274:22907-10.
57. Meagher J, Zellweger R, Filgueira L. Functional dissociation of the basolateral transcytotic compartment from the apical phago-lysosomal compartment in human osteoclasts. J Histochem Cytochem 2005;53:665-70.
58. Hayman AR, Jones SJ, Boyde A, et al. Mice lacking tartrate-resistant acid phosphatase (Acp 5) have disrupted endochondral ossification and mild osteopetrosis. Development 1996;122:3151-62.
59. Angel NZ, Walsh N, Forwood MR, Ostrowski MC, Cassady AI, Hume DA. Transgenic mice overexpressing tartrate-resistant acid phosphatase exhibit an increased rate of bone turnover. J Bone Miner Res 2000;15:103-10.
60. Vincent JB, Averill BA. An enzyme with a double identity: purple acid phosphatase and tartrate-resistant acid phosphatase. FASEB J 1990;4:3009-14.
61. Bresciani R, Von Figura K. Dephosphorylation of the mannose-6-phosphate recognition marker is localized in later compartments of the endocytic route. Identification of purple acid phosphatase (uteroferrin) as the candidate phosphatase. Eur J Biochem 1996;238:669-74.
62. Ek-Rylander B, Flores M, Wendel M, Heinegard D, Andersson G. Dephosphorylation of osteopontin and bone sialoprotein by osteoclastic tartrate-resistant acid phosphatase. Modulation of osteoclast adhesion in vitro. J Biol Chem 1994;269:14853-6.
63. Mundy GR, Bone Remodeling and Its Disorders In: I. Fogelman, eds. Metabolic Bone Disease. 1 ed. London, United Kingdom: Martin Dunitz Ltd, 1995:1-11.

64. Graves DT, Jiang Y, Valente AJ. The expression of monocyte chemoattractant protein-1 and other chemokines by osteoblasts. Front Biosci 1999;4:D571-80.
65. Zhao C, Irie N, Takada Y, et al. Bidirectional ephrinB2-EphB4 signaling controls bone homeostasis. Cell Metab 2006;4:111-21.
66. McBeath R, Pirone DM, Nelson CM, Bhadriraju K, Chen CS. Cell shape, cytoskeletal tension, and RhoA regulate stem cell lineage commitment. Dev Cell 2004;6:483-95.
67. Mundy GR, Elefteriou F. Boning up on ephrin signaling. Cell 2006;126:441-3.
68. Frattini A, Orchard PJ, Sobacchi C, et al. Defects in TCIRG1 subunit of the vacuolar proton pump are responsible for a subset of human autosomal recessive osteopetrosis. Nat Genet 2000;25:343-6.
69. Kornak U, Schulz A, Friedrich W, et al. Mutations in the a3 subunit of the vacuolar H(+)-ATPase cause infantile malignant osteopetrosis. Hum Mol Genet 2000;9:2059-63.
70. Michigami T, Kageyama T, Satomura K, et al. Novel mutations in the a3 subunit of vacuolar H(+)-adenosine triphosphatase in a Japanese patient with infantile malignant osteopetrosis. Bone 2002;30:436-9.
71. Scimeca JC, Quincey D, Parrinello H, et al. Novel mutations in the TCIRG1 gene encoding the a3 subunit of the vacuolar proton pump in patients affected by infantile malignant osteopetrosis. Hum Mutat 2003;21:151-7.
72. Chalhoub N, Benachenhou N, Rajapurohitam V, et al. Grey-lethal mutation induces severe malignant autosomal recessive osteopetrosis in mouse and human. Nat Med 2003;9:399-406.
73. Borthwick KJ, Kandemir N, Topaloglu R, et al. A phenocopy of CAII deficiency: a novel genetic explanation for inherited infantile osteopetrosis with distal renal tubular acidosis. J Med Genet 2003;40:115-21.
74. Ramirez A, Faupel J, Goebel I, et al. Identification of a novel mutation in the coding region of the grey-lethal gene OSTM1 in human malignant infantile osteopetrosis. Hum Mutat 2004;23:471-6.
75. Pangrazio A, Poliani PL, Megarbane A, et al. Mutations in OSTM1 (grey lethal) define a particularly severe form of autosomal recessive osteopetrosis with neural involvement. J Bone Miner Res 2006;21:1098-105.
76. Maranda B, Chabot G, Decarie JC, et al. Clinical and cellular manifestations of OSTM1-related infantile osteopetrosis. J Bone Miner Res 2008;23:296-300.

77. Campos-Xavier AB, Saraiva JM, Ribeiro LM, Munnich A, Cormier-Daire V. Chloride channel 7 (CLCN7) gene mutations in intermediate autosomal recessive osteopetrosis. Hum Genet 2003;112:186-9.

78. Shah GN, Bonapace G, Hu PY, Strisciuglio P, Sly WS. Carbonic anhydrase II deficiency syndrome (osteopetrosis with renal tubular acidosis and brain calcification): novel mutations in CA2 identified by direct sequencing expand the opportunity for genotype-phenotype correlation. Hum Mutat 2004;24:272.

79. Balemans W, Van Wesenbeeck L, Van Hul W. A clinical and molecular overview of the human osteopetroses. Calcif Tissue Int 2005;77:263-74.

80. Van Hul E, Gram J, Bollerslev J, et al. Localization of the gene causing autosomal dominant osteopetrosis type I to chromosome 11q12-13. J Bone Miner Res 2002;17:1111-7.

81. Van Wesenbeeck L, Cleiren E, Gram J, et al. Six novel missense mutations in the LDL receptor-related protein 5 (LRP5) gene in different conditions with an increased bone density. Am J Hum Genet 2003;72:763-71.

82. Benichou O, Cleiren E, Gram J, Bollerslev J, de Vernejoul MC, Van Hul W. Mapping of autosomal dominant osteopetrosis type II (Albers-Schonberg disease) to chromosome 16p13.3. Am J Hum Genet 2001;69:647-54.

83. Benichou OD, Laredo JD, de Vernejoul MC. Type II autosomal dominant osteopetrosis (Albers-Schonberg disease): clinical and radiological manifestations in 42 patients. Bone 2000;26:87-93.

84. Bollerslev J, Nielsen HK, Larsen HF, Mosekilde L. Biochemical evidence of disturbed bone metabolism and calcium homeostasis in two types of autosomal dominant osteopetrosis. Acta Med Scand 1988;224:479-83.

85. Bollerslev J, Steiniche T, Melsen F, Mosekilde L. Structural and histomorphometric studies of iliac crest trabecular and cortical bone in autosomal dominant osteopetrosis: a study of two radiological types. Bone 1989;10:19-24.

86. Waguespack SG, Koller DL, White KE, et al. Chloride channel 7 (ClCN7) gene mutations and autosomal dominant osteopetrosis, type II. J Bone Miner Res 2003;18:1513-8.

87. Del Fattore A, Peruzzi B, Rucci N, et al. Clinical, genetic, and cellular analysis of 49 osteopetrotic patients: implications for diagnosis and treatment. J Med Genet 2006;43:315-25.

88. Kovacs CS, Lambert RG, Lavoie GJ, Siminoski K. Centrifugal osteopetrosis: appendicular sclerosis with relative sparing of the vertebrae. Skeletal Radiol 1995;24:27-9.

89. Gerritsen EJ, Vossen JM, Fasth A, et al. Bone marrow transplantation for autosomal recessive osteopetrosis. A report from the Working Party on Inborn Errors of the European Bone Marrow Transplantation Group. J Pediatr 1994;125:896-902.

90. Berkelaar M, Clarke DB, Wang YC, Bray GM, Aguayo AJ. Axotomy results in delayed death and apoptosis of retinal ganglion cells in adult rats. J Neurosci 1994;14:4368-74.

91. Erben RG. Embedding of bone samples in methylmethacrylate: an improved method suitable for bone histomorphometry, histochemistry, and immunohistochemistry. J Histochem Cytochem 1997;45:307-13.

92. Cole AA, Walters LM. Tartrate-resistant acid phosphatase in bone and cartilage following decalcification and cold-embedding in plastic. J Histochem Cytochem 1987;35:203-6.

93. Kasper D, Planells-Cases R, Fuhrmann JC, et al. Loss of the chloride channel ClC-7 leads to lysosomal storage disease and neurodegeneration. EMBO J 2005;24:1079-91.

94. McCary LC, Smith CM, DeLuca HF. Hypophosphatemia and the development of rickets in osteopetrotic (op/op) mice. J Bone Miner Res 1997;12:1944-51.

95. Oliveira G, Boechat MI, Amaral SM, Young LW. Osteopetrosis and rickets: an intriguing association. Am J Dis Child 1986;140:377-8.

96. Miao D, Bai X, Panda DK, Karaplis AC, Goltzman D, McKee MD. Cartilage abnormalities are associated with abnormal Phex expression and with altered matrix protein and MMP-9 localization in Hyp mice. Bone 2004;34:638-47.

97. Tiffee JC, Xing L, Nilsson S, Boyce BF. Dental abnormalities associated with failure of tooth eruption in src knockout and op/op mice. Calcif Tissue Int 1999;65:53-8.

98. Cure JK, Key LL, Goltra DD, VanTassel P. Cranial MR imaging of osteopetrosis. AJNR Am J Neuroradiol 2000;21:1110-5.

99. Shapiro F, Glimcher MJ, Holtrop ME, Tashjian AH, Jr., Brickley-Parsons D, Kenzora JE. Human osteopetrosis: a histological, ultrastructural, and biochemical study. J Bone Joint Surg Am 1980;62:384-99.

100. Elster AD, Theros EG, Key LL, Stanton C. Autosomal recessive osteopetrosis: bone marrow imaging. Radiology 1992;182:507-14.

101. Li YP, Chen W, Liang Y, Li E, Stashenko P. Atp6i-deficient mice exhibit severe osteopetrosis due to loss of osteoclast-mediated extracellular acidification. Nat Genet 1999;23:447-51.

102. Chu K, Snyder R, Econs MJ. Disease status in autosomal dominant osteopetrosis type 2 is determined by osteoclastic properties. J Bone Miner Res 2006;21:1089-97.

103. Grodum E, Gram J, Brixen K, Bollerslev J. Autosomal dominant osteopetrosis: bone mineral measurements of the entire skeleton of adults in two different subtypes. Bone 1995;16:431-4.

104. Kobayashi T, Kronenberg H. Minireview: transcriptional regulation in development of bone. Endocrinology 2005;146:1012-7.

105. Pfeilschifter J, Diel I, Scheppach B, et al. Concentration of transforming growth factor beta in human bone tissue: relationship to age, menopause, bone turnover, and bone volume. J Bone Miner Res 1998;13:716-30.

106. Mundy GR. Peptides and growth regulatory factors in bone. Rheum Dis Clin North Am 1994;20:577-88.

107. Winkler DG, Sutherland MK, Geoghegan JC, et al. Osteocyte control of bone formation via sclerostin, a novel BMP antagonist. EMBO J 2003;22:6267-76.

108. van Bezooijen RL, Roelen BA, Visser A, et al. Sclerostin is an osteocyte-expressed negative regulator of bone formation, but not a classical BMP antagonist. J Exp Med 2004;199:805-14.

109. Poole KE, van Bezooijen RL, Loveridge N, et al. Sclerostin is a delayed secreted product of osteocytes that inhibits bone formation. FASEB J 2005;19:1842-4.

110. Bollerslev J, Marks SC, Jr., Pockwinse S, et al. Ultrastructural investigations of bone resorptive cells in two types of autosomal dominant osteopetrosis. Bone 1993;14:865-9.

111. Henriksen K, Sorensen MG, Nielsen RH, et al. Degradation of the organic phase of bone by osteoclasts: a secondary role for lysosomal acidification. J Bone Miner Res 2006;21:58-66.

112. Bollerslev J, Ueland T, Grodum E, Haug E, Brixen K, Djoseland O. Biochemical markers of bone metabolism in benign human osteopetrosis: a study of two types at baseline and during stimulation with triiodothyronine. Eur J Endocrinol 1998;139:29-35.

113. Semba I, Ishigami T, Sugihara K, Kitano M. Higher osteoclastic demineralization and highly mineralized cement lines with osteocalcin deposition in a mandibular cortical bone of autosomal dominant osteopetrosis type II: ultrastructural and undecalcified histological investigations. Bone 2000;27:389-95.

114. Senel K, Ugur M, Erdal A, Ozdemir H. Type II autosomal dominant osteopetrosis. Rheumatol Int 2002;22:116-8.

115. Taranta A, Migliaccio S, Recchia I, et al. Genotype-phenotype relationship in human ATP6i-dependent autosomal recessive osteopetrosis. Am J Pathol 2003;162:57-68.

116. Helfrich MH, Aronson DC, Everts V, et al. Morphologic features of bone in human osteopetrosis. Bone 1991;12:411-9.

117. Reeves J, Arnaud S, Gordon S, et al. The pathogenesis of infantile malignant osteopetrosis: bone mineral metabolism and complications in five infants. Metab Bone Dis Relat Res 1981;3:135-42.

118. Letizia C, Taranta A, Migliaccio S, et al. Type II benign osteopetrosis (Albers-Schonberg disease) caused by a novel mutation in CLCN7 presenting with unusual clinical manifestations. Calcif Tissue Int 2004;74:42-6.

119. Kornak U, Ostertag A, Branger S, Benichou O, de Vernejoul MC. Polymorphisms in the CLCN7 gene modulate bone density in postmenopausal women and in patients with autosomal dominant osteopetrosis type II. J Clin Endocrinol Metab 2006;91:995-1000.

120. Pettersson U, Albagha OM, Mirolo M, et al. Polymorphisms of the CLCN7 gene are associated with BMD in women. J Bone Miner Res 2005;20:1960-7.

121. Driessen GJ, Gerritsen EJ, Fischer A, et al. Long-term outcome of haematopoietic stem cell transplantation in autosomal recessive osteopetrosis: an EBMT report. Bone Marrow Transplant 2003;32:657-63.

122. Eapen M, Davies SM, Ramsay NK, Orchard PJ. Hematopoietic stem cell transplantation for infantile osteopetrosis. Bone Marrow Transplant 1998;22:941-6.

123. McMahon C, Will A, Hu P, Shah GN, Sly WS, Smith OP. Bone marrow transplantation corrects osteopetrosis in the carbonic anhydrase II deficiency syndrome. Blood 2001;97:1947-50.

124. Breast cancer and hormone replacement therapy: collaborative reanalysis of data from 51 epidemiological studies of 52,705 women with breast cancer and 108,411 women without breast cancer. Collaborative Group on Hormonal Factors in Breast Cancer. Lancet 1997;350:1047-59.

125. Sillero-Arenas M, Delgado-Rodriguez M, Rodigues-Canteras R, Bueno-Cavanillas A, Galvez-Vargas R. Menopausal hormone replacement therapy and breast cancer: a meta-analysis. Obstet Gynecol 1992;79:286-94.

126. Colditz GA, Egan KM, Stampfer MJ. Hormone replacement therapy and risk of breast cancer: results from epidemiologic studies. Am J Obstet Gynecol 1993;168:1473-80.

127. Thompson SG, Meade TW, Greenberg G. The use of hormonal replacement therapy and the risk of stroke and myocardial infarction in women. J Epidemiol Community Health 1989;43:173-8.

128. Wilson PW, Garrison RJ, Castelli WP. Postmenopausal estrogen use, cigarette smoking, and cardiovascular morbidity in women over 50. The Framingham Study. N Engl J Med 1985;313:1038-43.

Acknowledgement

I would like to express my gratitude to all those who gave me the possibility to complete this thesis.

I would like to thank the Department of Oral Surgery, Faculty of Dentistry of Chiangmai University, Thailand for giving me scholarship and permission to study doctorate in Germany for four years.

My former colleagues from the Department of Periodontology and the Department of Oral Surgery and Dental Radiology, Medical Faculty Charité, Campus Virchow, Berlin supported me in my preliminary work. I want to thank them for all their help, support, interest and valuable hints. Especially I am obliged to Dr. Nicole Pischon, Ms. Verena Kanitz, and Ms. Marion von Zitzewitz for technical counseling in basic laboratory work. I also would like to thank Dr. Gudrun Bethke, OA Dr. Frank P. Strietzel, OA Dr. Christian Scheifele for clinical skills and IT support during the early work.

Furthermore I have to thank colleagues from the Departments of Orthopaedics and of Trauma and Reconstructive Surgery, Center for Musculoskeletal Surgery, Charité-Universitätsmedizin Berlin, Ms. Gabriele Hardung, Mr. Martin Wolny, and Mr. Manav Mehta who advised me of technical assistance in histological procedure, picture analysis, as well as bone analysis by μCT.

I would like to express my gratitude to colleagues from the Institute of Medical Genetic, Charité-Universitätsmedizin Berlin, Mr. Jirko Kühnisch and Ms. Sabine Stumpp who instructed me in histological technique.

I am pleased to thank Dr. Jens Fuhrmann and Dr. Lena Wartosch who supported me material for the experiment and gave me an advice about gene expression analysis as well.

I want cordially to thank Prof. Dr. Stefan Mundlos and Prof. Dr. Thomas J. Jentsch who gave me permission to do research in their institutes and financial support.

I am deeply indebted to my research supervisor Dr. Uwe Kornak from the Institute of Medical Genetic, Charité-Universitätsmedizin Berlin whose help, stimulating suggestions and encouragement helped me in all the time of research for and writing of this thesis.

I would like to express my special thank to former head of the Department of Oral Surgery and Dental Radiology, Prof. Peter A. Reichart who gave me research consultation, looked closely at the final version of the thesis for English style and grammar, correcting both and offering suggestions for improvement, and is always of great help in difficult times.

Especially, I would like to give my special thanks to my father and mother whose patient love enabled me to complete this work.

CURRICULUM VITAE

Mein Lebenslauf wird aus datenschutzrechtlichen Gründen in der elektronischen Version meiner Arbeit nicht veröffentlicht

Erklärung an Eides statt

„Ich, Chayarop Supanchart, erkläre, dass ich die vorgelegte Dissertationsschrift mit dem Thema: „Characterization of the osteopetrotic Clcn7-/- mouse mutant rescued by osteoclast-specific expression of ClC-7'' selbst verfasst und keine anderen als die angegebenen Quellen und Hilfsmittel benutzt, ohne die (unzulässige) Hilfe Dritter verfasst und auch in Teilen keine Kopien anderer Arbeiten dargestellt habe."

Berlin, den 9. März 2009

Chayarop Supanchart